SPIN DEPENDENT TRANSPORT PROPERTIES OF GRAPHENE NANOANTIDOTS: A FIRST-PRINCIPLES STUDY

ALLAH DEKAMA

A thesis submitted to the school of graduate studies of Addis Ababa University in partial fulfillment of the requirements for the Degree of MSc in materials science

MATERIALS SCIENCE PROGRAM

COLLEGE OF NATURAL SCIENCES

ADDIS ABABA UNIVERSITY

ADDIS ABABA, ETHIOPIA

March, 2013

ADDIS ABABA UNIVERSITY

SCHOOL OF GRADUATE STUDIES

SPIN DEPENDENT TRANSPORT PROPERTIES OF GRAPHENE NANOANTIDOTS: A FIRST-PRINCIPLES STUDY

By Allah Dekama Jara

Materials Science Program

College of Natural Science

Approved by the Examining Board

Prof. Javed Mazher (Advisor) Signature _____ Date 12.03.2013

Dr. Ahmed Mustefa (Examiner) Signature _____ Date _____

Prof. TeketelYohannes (Examiner, Chairman) Signature _____ Date 19/03/2013

Abstract

Inherently, Graphene – a perfect 2D hexagonal crystal of C-atoms, is a non-spintronics material due to spin moment cancellation of C-atoms, especially, at the edges. Spintronics, or spin electronics, involves the study of active control and manipulation of spin degrees of freedom in the solid-state systems with non- equilibrium spin populations. The spins transport can be introduced either by doping or creating exotic nanostructures of graphene such as antidots. We have performed a systematic simulational study of bare and doped graphene nanostructures for their spin transport properties. We studied the transport properties of eight different D-shaped graphene nanoantidots (GNADs) with different electrode contact configurations by using non-equilibrium Green's functions (NEGF) in combination with the density-functional theory (DFT). Our calculations indicate the presence of spintronicity in the graphene nanoantidot's GNADs' geometrical conformations. Among the two important antidots (D_{1x} and D_{2x}), it is found that the former is more spintronic in comparison to the latter structure. Surprisingly, D_{2x} becomes more spintronic when the device is connected asymmetrically to its electrodes. This spin flip behavior is suitably explained in the thesis on the basis of zigzag edge spin-charge contributions to the devices. We have also studied effect of the presence of Co atom at center of GNAD on its spintronicity -- by comparing spin up and spin down conduction channels. The prospects of spin control among graphene nanostructures for spintronics applications are also discussed in the thesis.

Acknowledgements

I would like to express my sincere gratitude to Prof. Javed Mazher for being such an extraordinary supervisor. His unique and genuine enthusiasm for science kept me motivated during every step of my MSc, and in addition to supporting my core research activities he took the time and interest to educate me on a wide variety of other aspects about the scientific community and what it takes to succeed. I could not imagine a better MSc experience than having the privilege to work with and learn from Prof. Javed Mazher.

My thanks go to Prof. Teketel Yohannes, Chair of Materials Science Program college of Natural Sciences Addis Ababa University for introducing me to "spintronics" and initiate me to prepare seminar on "spintronics" when he provide me the course research method which motivate me to do research on the particular area.

Thanks are due to those who have had the pleasure of sharing computational laboratory of Materials Science Program with me: Assefa Abadi, Gishu Semu, and Solomon Teklehaymanot. They have all made my academic life at the Addis Ababa University much more interesting than it would have been on my own. Finally, I thank my family for their love and support, without which I would never have got here in the first place.

Table of Contents:

List of Figures

List of Tables

CHAPTER ONE

1. Introduction

The rapidly developing field of nanoscience has revealed new physical phenomena and encouraged the development of novel technological applications. The observance of ferromagnetic behavior among the C-atoms arranged in zigzag chain of the graphene nanostructures is one of such manifestations of nanotechnology. Nevertheless, most of the regularly shaped graphene nanostructures do not show any spin unbalance [1]. For instance, the ferromagnetic zigzag edges of one dimensional graphene nanoribbons are spontaneously coupled antiferromagnetically due to their opposite orientation and hence the net spin polarization effect is zero, However if we cut the edges or dope the ribbons, then there is the possibility to disturb such Antiferromagnetically AFM coupling, which could even results in strong spin polarization. We present a first-principles study of spin dependent transport properties of various exotic graphene nanostructures using Non-Equilibrium Greens Function Density Functional Theory (NEGF-DFT).

Graphene, a single-layer graphite sheet is a zero bandgap semi-conductor. It has attracted tremendous interests of theoretical and experimental studies due to high electrons mobility and long coherence length which are mandatory for nanoscale electronic and spintronics applications, even for the realization of room-temperature ballistic dissipation-free electronics. These and other unusual electronic properties of graphene make it a promising material for building spintronics devices. Nevertheless, absence of magnetism in graphene sets limitations on its practical spintronics applications. Thus it is of crucial importance to find methods to effectively introduce and tune the electric spin

passing in graphene for broadening its applications in nanospintronics. In this work we have created two different types of D-shaped graphene nanoantidots (GNAD) for the purpose of intensive study of their spin dependent transport properties with and without spin dopants by using first principle ab-initio DFT techniques along with spin polarized Local density approximation (SLDA).

The content of the thesis can be summarized as follows. In the first chapter we provide an overview of graphene nanostructures for spintronics applications. Chapter 2 is objectives of the study. In the Chapter 3 the theoretical framework and the methodology used to achieve the objectives of this research will be explored. Finally, we will discuss about the findings and results obtained from the modeling and simulation. In addition to this the result achieved based on the objectives of the research is summarized in Chapter 4.

1.1 Graphene

Graphene is one of the allotrope of carbon atoms in which electrons of carbon atom occupy the atomic orbitals of $1s^2 2s^2 2p^2$. The electrons in the $1s^2$orbital are called core electrons, they are strongly bonded. The four remaining electrons are valence electrons and are distributed to more delocalized orbitals. The energy difference between the 2s and the 2p level is much smaller than their binding energy, thus the wave functions of these four electrons can mix up easily by the hybridization process to form sp^2 hybrid orbital. After this process three σ states lie in the xy-plane and draw an angle of 120^0. The σ states form covalent bonds with their neighbors and give rise to the hexagonal lattice structure of graphene [2]. The remaining state, $2p_z$ orbital is aligned in the

z-direction and form π states. Electrons in π state are weakly bonded and can hop easily between neighboring atoms and play an important role for the transport properties.

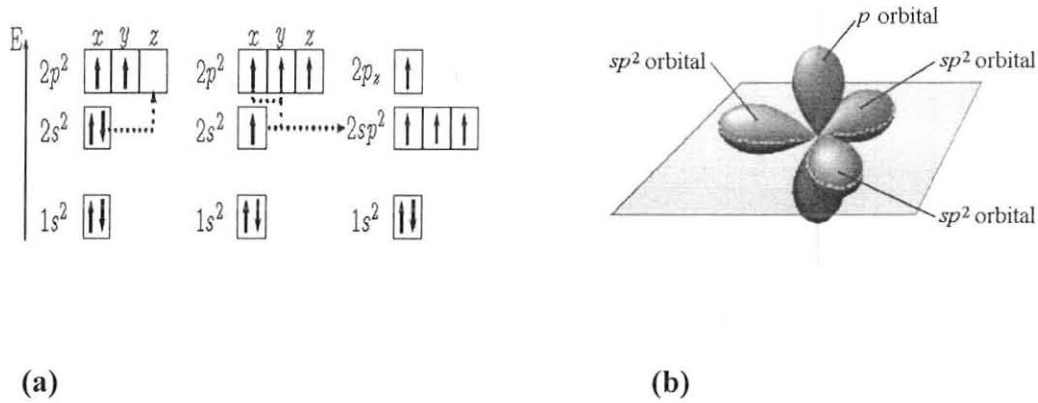

(a) **(b)**

Figure 1.1: Schematic diagram of sp^2 hybridization of graphene. (a) The structure of orbital after the hybridization. (b) Angular distribution among the π and σ orbitals [3].

Graphene is a single atomic layer of graphite produced by mechanical exfoliation of graphite [3]. The carbon atoms in graphene are arranged in a hexagonal lattice and are covalently bonded. The covalent σ bond provides strong binding between the carbon atoms, but the corresponding electrons contribute poorly to the conductivity. The one half-filled p_z orbital left on each carbon atom, is orthogonal to the graphene plane after forming covalent bond with the neighbor atoms, as in Figure 1.1 (b). The interaction of the p_z orbitals residing on the nearest-neighboring carbon atoms results in the generation of the π bonds below and above the graphene plane. The π electrons are delocalized across the entire lattice and contribute to the conductivity of graphene.

1.2 The Crystal Structure of Graphene

In a graphene layer the carbon atoms are distributed at the edges of regular hexagons structure called Honey comb as depicted in Figure 1.2 (a).

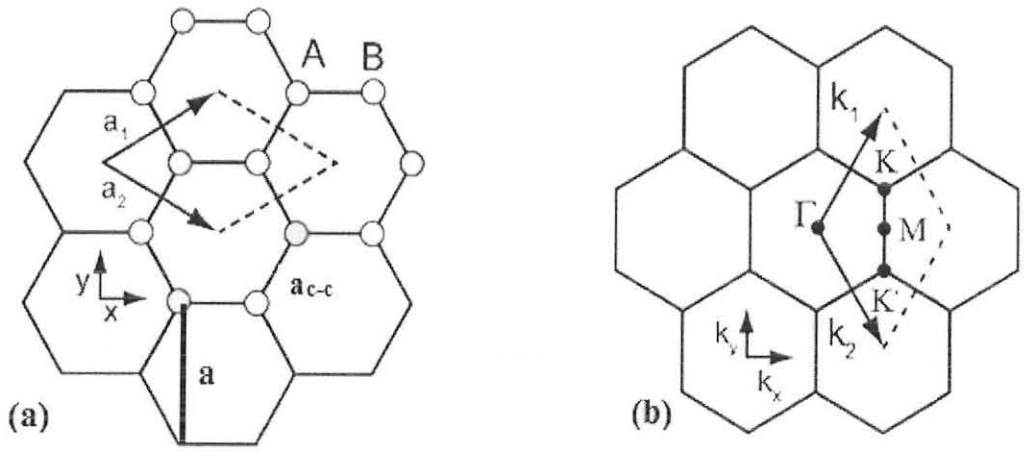

Figure 1.2: (a) Real space unit cell of graphene. The real space lattice vectors a_1 and a_2 define the graphene unit cell (grey shaded rhombus), which contains two carbon atoms, each belonging to two intersecting sublattices, A and B. (b) The first Brillouin zone (BZ) of graphene (grey shaded) with the high-symmetry points (Γ, M, K, and K') [4].

The two atoms of primitive unit cell are often referred to as A and B atoms. The unit cell of the lattice is a rhombus defined by the two vectors a_1 and a_2, as:

$$a_1 = \sqrt{3}\, a_{c\text{-}c} \left(\frac{\sqrt{3}}{2}, \frac{1}{2}\right), \qquad a_2 = \sqrt{3}\, a_{c\text{-}c} \left(\frac{\sqrt{3}}{2}, -\frac{1}{2}\right) \tag{1.1}$$

$$a = |a_1| = |a_2| = \sqrt{3}\, a_{c\text{-}c} \tag{1.2}$$

where $a_{c\text{-}c} = 0.142$ nm is interatomic distance. Interatomic distance and lattice constant are related as: $a = \sqrt{3}\, a_{c\text{-}c}$ where "a" is a lattice constant.

And the k-vectors shown in Figure1.2 (b), are given by

$$k_1 = \left(\frac{2\pi}{\sqrt{3}\, a_{c\text{-}c}} (1/\sqrt{3}, 1), \right) \text{and, } k_2 = \left(\frac{2\pi}{\sqrt{3}\, a_{c\text{-}c}} (1/\sqrt{3}, -1) \right) \tag{1.3}$$

Out of the six corners of this Brillouin zone only two are inequivalent positions, since the others can be obtained from an elementary translation of the form $nb_1 + mb_2$, where n and m are integers. These inequivalent corners or symmetry points are commonly denoted as K and K' [5, 6]. In the reciprocal space, the two-atom unit cell results in a Brillouin zone with two conical points at the Fermi surface, K and K' (often referred to as the Dirac points) as illustrated in Figure 1.3 (b) where the π - and π^* -bands touch each other. In the vicinity of these points, the electron energy is linearly dependent on the wave vector. Consequently, graphene is a special semi-metal or a zero-gap semiconductor. In conventional semiconductors, the electrons at band edges usually obey a quadratic energy-momentum relation [7]. The electronic properties of graphene are best described by an equation of the form of the relativistic Dirac equation rather than the non-relativistic Schrodinger equation due to this unique linear dependence [2].

The band structure of graphene can be understood through the dispersion relation, which is given in Figure 1.3 (a). When well separated atoms are brought together to form a crystal then the charge distribution of adjacent atoms overlaps and that is responsible for the changes in the atomic energy level and the mutual interaction between the nearest neighbors.

In the Figure 1.3 (b) the corner of the hexagonal first Brillouin zones represent the meeting point of valance and conduction band which is called as Dirac point and the

corresponding energy is called charge neutrality point [3]. The dispersion relation around the K and K' points is linear, and is given by

$$E = |\hbar k| \upsilon_f \tag{1.4}$$

Thus charge carriers in graphene mimics the case of mass less relativistic particle and the dispersion relation can also be written from Einstein's relativistic equation:

$$E = \sqrt{(m^2c^4 + p^2c^2)}\ , \text{if}\ , m = 0, E = pc \tag{1.5}$$

The equations (1.4) and (1.5) lead to conclusion that $E = \hbar kc$ [9] where the electrodynamics in graphene is effectively relativistic for speed of light c that is substituted by Fermi velocity υ_f .

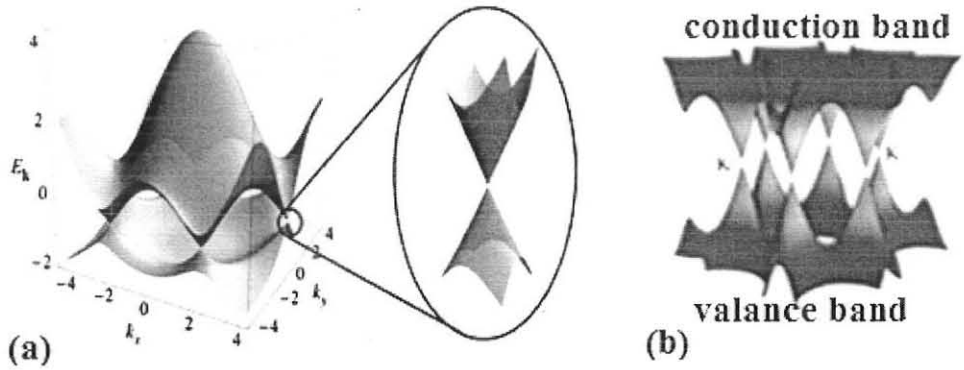

Figure 1.3: Electronic dispersion in the honeycomb lattice (a) Left: energy spectrum around the six Dirac cones. Right: zoom shows the energy bands close to one of the Dirac points. (b) π- π*- band structure of graphene [3].

These π bands meet and become cone shaped at the K-points such that they are degenerate and display a linear dispersion near the K-points resulting in zero effective mass for electrons and holes and induces high mobility of the charge carriers.

1.3 Important Characteristics of Graphene

Graphene with its unique nanoscale properties has opened the door to possibly substitute it for silicon for the next generation of electronics. Some of the promising properties of graphene [10-19] and its application in large number of emerging technologies are shown in the table 1.1.

Table 1.1 Graphene unique properties and its breakthrough application.

Properties	**Applications**
High room temperature mobility (~200,000 $cm^2V^{-1}s^{-1}$)	Electronics (RF, MEMS), silicon replacement
High strength (Elastic modulus ~1 TPa)	Composite materials
High surface/weight ratio	Energy storage (fuel cells)
High light transparency	Transparent electrodes
High sensitivity for chemicals	Chemical/bio sensors
High thermal conductivity	Heat/energy storage, thermal management
Magnetic nanostructures	Spintronic devices

1.4 Graphene Nanostructures and their Electronic Properties

High electron mobility and their long coherence length make graphene a subject of great interest for nanoscale electronic applications, even for the realization of room-temperature ballistic dissipation free electronics [4, 20]. However, a major drawback in the development of graphene based devices industry is the failure of electrostatical confinement of electrons in the graphene, because a single layer of graphite remains metallic even at the charge neutrality point. In order to overcome this problem, a way to open a gap in the electronic structure of graphene has to be found. A straightforward

solution is to pattern graphene sheet into narrow novel nanostructures such as graphene nanoribbons, quantum dots, and antidots made by graphene [21-23].

The graphene nanoribbons (GNRs) are elongated strips of graphene with a finite width that can be obtained by cutting a graphene sheet along a certain direction [24, 25]. Due to the honeycomb structure of graphene, two prototypical shapes are possible for the edges, namely the armchair edge and the zigzag edge [6, 24 - 26] which are shown in a Figure 1.4. Depending on the cutting direction, the edges of the GNRs may thus exhibit either one of these two "ideal" shapes or more complex geometries composed of a mixture of armchair and zigzag shaped fragments with their corresponding unit cells.

Unusually, the GNRs with armchair (zigzag) edges on both sides are classified by the number N of dimer (zigzag) lines across the ribbon width, as illustrated in Figure 1.4 [4]. For stability the GNR dangling bonds on the edge sites of GNRs are usually terminated by hydrogen atoms [27], although dangling bonds would not make any significant contribution to the electronic states near the Fermi level [4]. Theoretical calculations and experiments have shown that the electronic and transport properties of GNRs are strongly influenced by the actual atomic configuration of the edges, which, contrary to bulk graphene, are very reactive. A detailed knowledge of the stability and electronic properties of the different types of edges is therefore required in order to understand and ultimately design GNRs with specific properties [28].

An armchair ribbon is cut so that the edge looks as if it consists of repeated armchairs, as shown in Figure 1.4 (a). Each edge is terminated by atoms of the A- and B-sublattice. The width of an armchair ribbon can be defined in terms of the number of dimer lines.

The other basic edge geometry is the so called zigzag edge, shown in Figure 1.4 (b). The atoms at one edge are of the same sublattice, for instance A atoms at the left edge and B atoms at the right edge. The width of a zigzag ribbon is now identified with the number of zigzag chains N_{ZZ}, as

$$W_{ZZ} = (N_{ZZ} - 1)\frac{3}{2}a_{c\text{-}c} \tag{1.6}$$

where $a_{c\text{-}c} = 1.42\,\text{Å}$ the nearest neighbor distance.

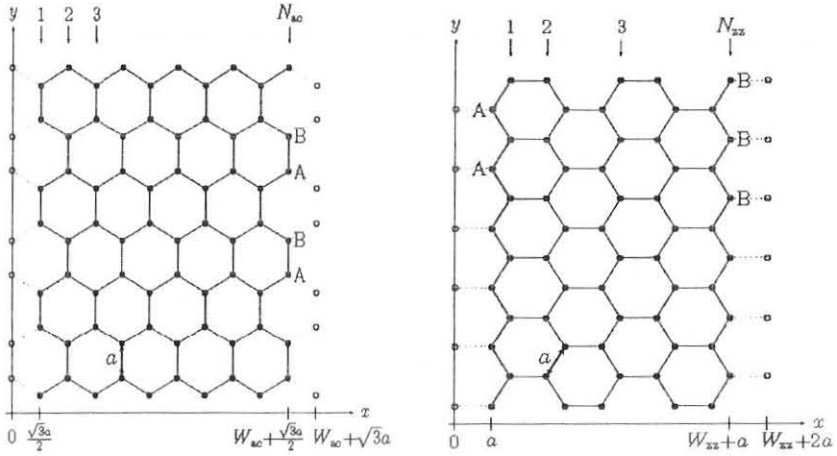

Figure 1.4 Lattice structures of graphene nanoribbons. The dotted lines show the bonds that have to be cut and the circles show the atoms that have to be removed in order to create (a) an armchair nanoribbon (the one to left). (b) a zigzag nanoribbon (to the right).

The width of an armchair ribbon is also identified with the number of dimer chains (N_{ac}) as

$$W_{ac} = (N_{ac} - 1)\frac{\sqrt{3}}{2}a_{c\text{-}c} \tag{1.7}$$

where $a_{c\text{-}c} = 1.42\,\text{Å}$ the nearest neighbor distance.

1.4.1 Graphene Nano AntiDots (GNADs)

Very recently an interesting fact has been noticed about these graphene nanostructures which imply that a magnetic character can be induced amongst them on breaking the edge symmetry.

(a) 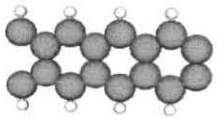 (b) 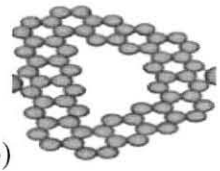

Figure 1.4.1 (a) A graphene nanostructure with symmetric edges and showing zero spin transport. (b) A graphene nanostructure with asymmetric edges and also a hollow dot (anti region) at the center, which is believed to show spin transport.

For instance, from the first principles calculations it has been found that the symmetric ribbons of graphene do not transport spin but the ribbons with antidots in them can transport electron spin. The details are further mentioned in Section 1.6.

1.5 Transmission and density of states DOS among GNR

As described in Section (1.4), GNRs have unique electronic properties; they become either metallic or semiconducting as a function of ribbon width. Thus GNRs show distinct electronic properties when compared to pure two-dimensional graphene. However, zGNRs are mostly metallic but their density of states decreases with width. In addition, recent reports have also found that zGNR with irregular shapes are magnetic due to spin polarization effects found in the edges of ribbons. Nevertheless, aGNR is metallic only if the number of rows of carbon is 3M−1, where M is an integer [29]. On reducing the structure along the length, and hence going from one to zero dimensions, one confines edge states by terminating the length dimension. It is also showed that the

electronic structure of zero-dimensional armchair graphene nanoribbons has a length dependence of electronic states for certain widths, which varies greatly from the one-dimensional results, as calculated with density functional theory. For the ribbons of the same width the bandgap is smaller for the longer ribbons. Thus the density of state near the Fermi energy decreases for shorter length ribbons.

The transport properties of graphene nanoribbon are mostly determined by the electronic states presented around the Fermi energy exactly in between the K and K' points. Around these points, the electronic states are described by a linear dispersion relation. As a consequence, charge carriers in graphene nanostructure have some unique transport properties, like an anomalous quantum Hall effect [4, 10] and a minimum conductivity at the charge neutrality point. Most importantly the spin dependent transmission in which only one type of spin is allowed to be transferred across the GNR nanostructure is found to have large spin coherence lengths in this perfect 2D crystal [30]. Furthermore, graphene exhibits very high electron and hole mobility's [3], exceeding 2×10^5 cm^2 V^{-1} s^{-1} at room temperature which paves the way for a fast interplay for spin transmission dynamics. In addition, aGNRs in quantum dot configuration are also found to be magnetic due to the zigzag terminated length-confined edges. Hence zigzag edges are crucial from spintronics point of view. Experimentally, it has been found that graphene ribbons of finite lengths have the same effects on the magnetic properties of nanoribbons and thus the spin energy bandgap depends both on the width and lengths of the ribbon. The spintronics property of any device is usually evaluated by the extent to which it polarizes the spin current [31]. Energy dependent relative spin polarization of the transmission probabilities is given by,

$$P = \frac{(T_{\uparrow} - T_{\downarrow})}{(T_{\uparrow} + T_{\downarrow})} \tag{1.8}$$

where $T_{\uparrow}$ and $T_{\downarrow}$ are the transmission of spin up and spin down electrons respectively. The conductance of the spin channels is also given by

$$G(E) = G_0 \sum T(E) \tag{1.9}$$

Where $G_0 = 2e^2/h$ is conductance quantum.

1.6 Magnetic and Spintronic Properties of Graphene

Zigzag graphene nanoribbons have so-called edge states. According to numerous theoretical studies based on density functional theory, it is found that the zigzag patterned carbon atoms are ferromagnetically ordered along one edge, and antiferromagnetically ordered between opposite edges [13]. For the perfectly rectangular ribbon, these two magnetisms are exactly equal and they cancel out each other. This antiferromagnetic ground state is consistent with the **Lieb's theorem** [32], which states that the total spin of the ground state is $1/2|N_B\text{-}N_A|$ such that N_A (or N_B) is number of edge atoms on the two A and B triangular sub-lattices of the graphene. Thus the perfect zigzag ribbon is nonmagnetic. Nevertheless, if we cut off the ribbon in irregular shapes such that parallelism of the FM edges gets disturbed. Then the antiferromagnetic (AFM) effect would not be complete and owing to the partial FM cancellation we get some remnant magnetism in the ribbon edge. This is the origin of the introduction of just one form of the magnetism in zGNR. Similarly, we can also introduce magnetism by doping the ribbon with magnetic ad-atoms like Co, Mn, etc. due to the presence of unpaired electrons in these atoms. The phenomenon of edge magnetism is not restricted to ideal

zGNRs but is believed to occur in any graphene system that has zigzag edge segments. Previously researchers suggested the use of magnetic zigzag edges for spintronics applications [6]. They showed that the application of a transverse electric field causes the antiferromagnetic zGNRs to become half-metallic because of the flipping of magnetic moments in the direction of applied field. Without an electric field, the system is found to be in the antiferromagnetic ground state with a bandgap at E_F. The external electric field shifts the electronic states so that the bandgap of one spin component is increased [33] while the bandgap of the other spin component is closed, such that the system becomes a metal with spin-polarized electrons, such a GNR device is also called as a spin valve because it effectively allows the transport of only one type of spin electrons and completely blocking the flow of other spin depending up on its intrinsic facilitation for the former spin. In essence, the effect of the transverse electric field is to break the symmetry between the left and the right edge. This symmetry breaking can be achieved without an electric field also in different ways which is the main purpose of our thesis research, for example, by saturating the left and the right edge of the zGNR with different ad-atoms or by creating edge selective anti regions [31,34]. Another interesting hybrid method is to introduce spintronicity by the application of magnetic atom doping [35]. More recently it has also been reported that a different type of intrinsic magnetism can be induced by certain types of point defects in bulk graphene. Point defects are, for example, lattice vacancies (missing carbon atoms) [36]. Similar to edges, a point defect interrupts the ideal sp^2 lattice structure and induces electronic states that can be magnetic for instance at room temperature. Furthermore, magnetic properties can be induced by foreign magnetic atoms that are either adsorbed to graphene or replace carbon atoms in

the honeycomb lattice [37, 38]. It is worth to mention that there are certain set of rules for the modification of edge states of GNRs to induce spintronicity, which we have also followed in this thesis work during the modality of spintronics samples. Researchers who are working in this field often refer these rules as the spintronicity design rules which are described below.

1. The first design rule is a simple geometric rule which states that the magnetism of all GNR materials depends on the ground state magnetic ordering within a single nanoribbon, nanodot, or nanohole and this ordering is consistent with the Lieb's theorem of itinerant magnetism in a bipartite lattice. The theorem also explains that the graphene consists of two atomic sublattices (A and B), and a zigzag edge must be either on an A- or B-sites of the lattice for reading the FM behaviour. It is found that in a given GNR, two edges will be FM-coupled if they are on the same sublattice and AF-coupled if they are not. Thus the total spin S of the ground state equals to the value of $1/2|N_B-N_A|$, where N_B (N_A) is the number of atoms on the B (A) sublattice [32, 39].
2. The second design rules is also edge symmetry based which says that owing to the underlying honeycomb lattice symmetry, the relationship between any two zigzag edges is uniquely defined by their relative angle to each other. Specifically, atoms on the same zigzag edge belong to the same sublattice either A-lattice or B-lattice. If the atoms on two different zigzag edges belong to the same sublattice then the two edges should be at an angle of 0° or 120° to each other in order to show spintronicity. But if the atoms are at different sublattices then they are at an angle of 60° or 180° to each other in order to show non-spintronicity. Using this we can

say that any two zigzag edges are FM-coupled if they are at an angle of 0° or 120° and AF-coupled if they are at an angle of 60° or 180° [39, 40]. The rule partially reflects the three-fold rotational symmetry of the graphene honeycomb lattice and the reflection symmetry between the two sub-lattices. Note that the angle between any two edges can also be defined formally as the angle between the two normal vectors of the edges.

3. Along with the type of edges and their angular pattern, very recently a novel rule is also introduced for graphene nanostructures. According to this rule we can introduce spintronicity just by disturbing the axial alignments of the electrode contacts on the graphene nanostructures [30]. For instance if there is some asymmetry in between the left and right electrode contact on the central region of the graphene spin device, it is said that either the spin current enhanced or a new spintronicity is introduced among the normal. The magnetic ground states of the nanodots modelled by spintronicity rules are already found to be consistently magnetic by existing first principles calculations for all different shapes of nanoantidots [39,]. Also, the same is true for individual antidotes punched in graphene thus it has been found that only the FM nanodots have a net magnetic moment, while AF nanodots have zero moment which is the clear validation for the said design rules [40]. For magnetic and spintronics applications, it is desirable to search for FM nanoantidots with a net moment as high as possible. This is the aim of the present thesis research work. In this thesis we have modelled a very new D-shaped antidots based on the above designed rules. With the aid of a generic design rule, our search becomes much easier. It should be

noted that as the rule suggests, the first key to the design is to eliminate edges which are at 60° or 180° to each other, so that the nanodots contain only edges which are at 0° or 120° to each other and they all have the same spin orientation. The second key is to elongate the edge length as much as possible to maximize the total net moment. The design rule is also explained schematically in Figure 1.5 which gives more light on the origin of spintronicity in these novel graphene nanostructures. Figure 1.5shows that all the inner edges of triangular antidot are at same sublattice (red) and120° to each other – the signature of presence of spintronicity in the antidot.

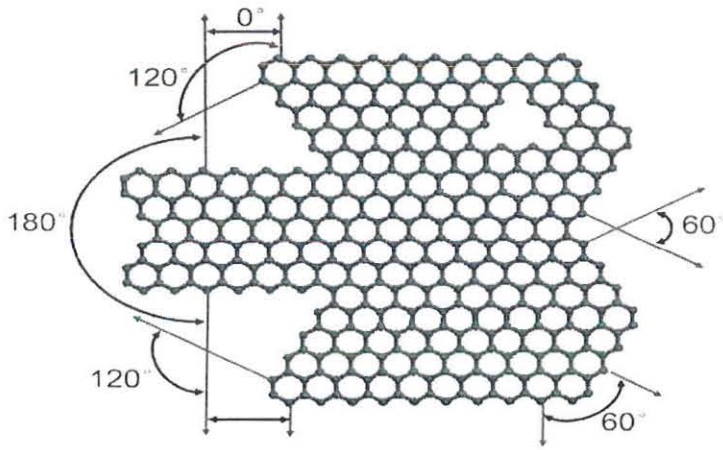

Figure 1.5 Schematic illustration of the underlying geometric relationship between zigzag edges in graphene. It illustrates that the edges are on the same sublattice {A (red, topmost atom line) or B (blue, bottommost atom line)} are FM coupled -- if they are at an angle of 0° or 120° to each other--and on different sublattices are AFM coupled at an angle of 60° or 180°[40].

Just like in zGNRs, magnetism can also be formed in graphene dots with zigzag edges. In a graphene molecule with rectangular or hexagonal edges, magnetic moments with the

same magnitude and different signs are always formed on the two opposite zigzag edges. Thus the total spin S_t in such systems is exactly zero. However, in a molecule with triangular zigzag edges, exactly the same magnetic moments are observed on all edges. So the total spin S_t is nonzero. Like in zGNRs, the local magnetism in graphene dots arises from the spin-polarized edge states localized on the zigzag edges [13, 40]. In the end, we can say that aforementioned logic can be applied to explain the origin of magnetism in the antidots of graphene nanoribbons (GNR). Graphene dots are just graphene molecules with finite size in all directions while antidots are structures with holes in graphene with some kinds of dots cut away from it. Hence it would be interesting to explore the dependency of spintronicity on the product of graphene nanoantidot (GNADs) size and density (ρ) for the small size limit of GNADs. Also the spin bandgap increases linearly with the increasing product of antidots size. This simple scaling rule can be useful in the future design of magnetic super lattices made up of nanodots as integrated circuits (ICs) for their potential applications in graphene-based nano electronics and spintronics.

1.7 Difficulties in commercialization of Graphene based spintronics

Despite of the recent invention of wafer size graphene substrates, much optimization is needed to prepare high-quality, large area graphene sheets suitable for industrial applications for spin logic, the spintronics design rules used to introduce spintronicity is also works for only a certain specific geometry; moreover an accurate control of individual features like spin density of state (SDOS) and spin transmission in graphene nanostructures spin devices are still a challenge for both theoreticians and experimentalists. Structures, due to contribution of the inner anti-edges of the antidots

towards promoting the antiferromagnetic comply. It is imperative to explore further causes of FM comply among these antidots (ADs). Due to these and other, commercializing graphene as a spintronics device is not practical at this moment.

CHPTER TWO

2.1 Objectives

The general and specific objectives of this work are given below.

2.2 General Objectives

- To study the exotic graphene nanostructures for spintronic devices.

2.3 Specific Objectives

- To design D-shaped graphene nanoantidots (GNADs).
- To investigate the bare antidot in mixed armchair and zigzag graphene nanoantidot a/z(GNAD) configuration and to compare their spin transport properties.
- To study the effects of cobalt as spin dopant in different antidot configurations.
- To simulate the spin transport properties of exotic graphene D type antidot nanostructures in different contact electrode configurations at different gating levels.

CHAPTER THREE

3. Methodology and Simulation

3.1 Theoretical Framework

Determination of the electronic structure of solids is a many body problem that requires a Schrödinger equation to be solved for an enormous number of nuclei and electrons (typically 10^{23}).

$$\hat{H}\ (r) = (\hat{T} + \hat{V}_{e-e} + \hat{V}_{e-i} + \hat{V}_{i-i}) \qquad (3.1)$$

Here r denotes the positions and spins of the electrons, i.e., $(\mathbf{r}_1; s_1; \mathbf{r}_2; s_2; \ldots)$, $\hat{T}$ is the kinetic energy operator, $\hat{V}_{e-e}$ is the columbic electron-electron repulsion $\hat{V}_{e-i}$ is the columbic ion electron interaction and $\hat{V}_{i-i}$ is the interaction between ions.

Also it is complicated to apply this solved wave function of a crystal in the calculation of physical observables, thus the exact solution of the many body problems is impossible. This is because theoretically we can describe physical quantity only with the help of energy spectrum or E-K curve and two to three correlation functions.

A fully quantum mechanical treatment of a nanoscale system requires confronting the many-body Schrödinger equation for all particles. Fortunately, in many physical problems, we can restrict our focus to just the electrons in the system. This is because electrons are much less massive than nuclei and so respond to forces much faster. In addition, the Born-Oppenhemier approximation which states that the wavefunction of the entire system (electrons and nuclei) is separable into an electron-only part and nuclei-only part. If the motion of the nuclei are needed, for instance when relaxing a nanoscale device structure, there are approaches that separate the dynamics of the electrons and

nuclei, thus preserving the theoretical and computational advantages of this approach. Even with the fixed-nuclei approximation, we still have a many-electron Schrödinger equation to solve. Solving this equation is impossible in all but simple systems, and the only way to make progress in realistic systems is to make approximations.

One of these approximations is the Hartree method, here the many-electron wave function Ψ is approximated as a product of N single-electron wavefunctions; and given by

$$\Psi(r_1, r_2, r_3 \ldots r_N) = \phi_1(r_1)\ \phi_2(r_2)\ \phi_3(r_3) \ldots \phi_N(r_N) \qquad (3.2)$$

where N is the number of electrons.

The Hartree-Fock method extends the Hartree approach by using an antisymmetrized product of single-electron wavefunctions. Slater showed that an elegant way to accomplish this is to arrange the single-particle wavefunctions in a determinant. The determinant enforces the antisymmetry requirement since interchanging a row or column of a determinant which is equivalent to exchanging the positions of the corresponding electrons and thus it changes the sign of the result. Both the Hartree and Hartree-Fock methods neglect electron correlations. Post Hartree-Fock methods are those approaches that include electron correlation effects. These methods which includes electron correlation effects are able to produce impressively accurate results, but at a high computational cost. Due to this, they are not presently practical for use in systems beyond a few tens of atoms. Nevertheless density functional theory (DFT) is the only viable way to handle much larger systems in an efficient manner. DFT assumes that there is just a single electron interacting in some potential and its solution is used to obtain the

observables corresponding to the actual many-electron system. In mathematics, a functional is a function that takes another function as its argument. The name "density functional theory" comes from the fact that various terms in the systems Hamiltonian can be expressed as functionals of the density, the electron density, $n(\vec{r})$, can be obtained from the wave function by integrating over all spatial coordinates.

$$n(\vec{r}) = N \int \ldots \int |\Psi(r_1, r_2, r_3 \ldots . r_N)|^2 \, dr_2 \ldots . dr_N \qquad (3.3)$$

The central idea of DFT is that one does not need to calculate the many-body wavefunction. Instead, the electron density, $n(\vec{r})$, is sufficient. The justification for this simplification comes from the Hohenberg-Kohn (HK) theorems. They prove that there is a one-to-one correspondence between the total electron density and the corresponding wave function (and therefore the potential). This means that the density contains the same information as the wavefunction, and so the observables can be calculated using just the density. This avoids the need to find the exact wavefunction.

The HK theorems establish that all one needs is the density, but do not give a method to obtain it. The Kohn-Sham (KS) method provides numerical procedure for this calculation. Consider a simpler problem, in which the electrons do not interact with each other. Each of these "independent" electrons moves in a potential that represents the properties of the system in an average way. This decoupled system's Hamiltonian is simpler to solve and results in eigenstates called as Kohn-Sham orbitals, ϕ_i. The KS method constrains these orbitals such that the density calculated from them matches the actual system's density, which is all that is needed to calculate system observables. On

using the effective potential in the Schrödinger equation we get the Kohn-Sham equations (one equation for each orbital). The minimum of the total energy functional is the ground state energy of the system and the density which gives this minimum is the exact single-particle density of the ground state. Thus the Kohn-Sham total energy function is

$$E[\phi_i] = 2\sum_i \int \phi_i \left(-\frac{\hbar^2}{2m} \right) \nabla_i^2 d^3r + \int U^{ION}(r)\, n(r)\, dr + \frac{e^2}{2} \int \frac{n(r)\, n(r')}{|r-r'|} dr dr' + E_{XC}[n(r)] + E_{nn} \tag{3.4}$$

where ϕ_i are electron states or KS orbitals.

$$E_{nn} = \sum_{ij} \frac{Z_i Z_j}{|R_i - R_j|} \tag{3.5}$$

E_{nn} is the energy due to mutual nuclear repulsion. Since we assume fixed nuclei, this energy is constant. U^{ION} is the electron-ion potential, n(r) is the electron density.

$$n(r) = 2 \sum_{i=1}^{N_{occupied}} |\Psi_i(r)|^2 \tag{3.6}$$

$\frac{e^2}{2} \int \frac{n(r)\, n(r')}{|r-r'|} dr dr'$ is the electron-electron repulsion and $E_{XC}[n(r)]$ is the exchange-correlation functional. It is to be noted that in Equation (3.5) the factor of 2 includes contributions from both up and down spins. Only the minimum of the energy functional has physical meaning, and at the minimum it gives the ground state energy of the system. At the minimum, the electronic states ϕ_i are self-consistent solutions of the Kohn-Sham equation given by

$$H_{KS}\,\phi_i(r) = E_i\,\phi_i(r), \quad H_{KS} = \left(-\frac{\hbar^2}{2m}\right)\nabla^2 + U^{KS}\left[n(r)\right] \qquad (3.7)$$

$$U^{KS} = U^{ION}(r) + U^{H}(r) + U^{XC}(r) \qquad (3.8)$$

where E_i is the Kohn-Sham eigenvalue, and U^H is the Hartree-potential of the electrons defined as

$$U^{H}(r) = \frac{e^2}{2}\int \frac{n(r')}{|r-r'|}\,dr' \qquad (3.9)$$

The exchange-correlation functional, U^{XC} is the functional derivative of the exchange-correlation energy.

$$U^{XC}(r) = \frac{\delta E_{XC}\left[n(r)\right]}{\delta\left[n(r)\right]} \qquad (3.10)$$

Note that the Hartree term U^H represents the Columbic interaction between a single electron and the density due to all other electrons. This density looks the same to all of the electrons, and so this avoids many-body complications.

Thus the KS approach represents the electron-electron Columbic interaction as a single electron interacting with an effective mean field. One problem with this over simplified approach is that in reality the electrons' movements are correlated and exhibit variety of interaction amongst their pair electrons. Consider a two-electron system; at the position of one electron, the probability of finding the other electron decreases, and *vice-versa*. Thus the mean field approximation does not take this behavior into account, and so it models a system of electrons that can get too close to one another. This is not possible; similarly exchanging the spatial and spin coordinates of two electrons must change the

sign of the many-body wavefunction. This leads to the Pauli principle, which causes electrons of like spins to avoid each other thus they are not in the same state. Unlike the correlation effect, this exchange effect only applies to electrons of like spins. Thus in KS approach the exchange-correlation (XC) term is induced in the potential and, U^{XC} is defined to contain the difference between the real and effective potentials, which are mainly quantum effects due to electron exchange and correlation.

The first and most simple approximation is the local density approximation (LDA). In the LDA the exchange-correlation energy is assumed to be

$$E_{XC}^{LDA} = \int \epsilon_{XC}\,[n(r)]\, n(r)\, dr \qquad (3.11)$$

where $\epsilon[n(r)]$ is the exchange-correlation energy per unit volume of a homogeneous electron gas of density n(r). Once the KS spin orbitals are determined, the total energy can be obtained from Equation (3.5) explores for exploring systems with exchange interactions, following from

$$E[\phi_i] = \sum_{i}^{N_{occup}} E_i + \int dr \left(\frac{1}{2} U^{H}(r) + U^{XC}(r) \right) n(r) + E_{XC}[n] + E_{nn} \qquad (3.12)$$

3.1.1 Spin Exchange Approximations

The main difficulty with local-density approximation (LDA) is that the functional depends only on the density at the coordinate where the functional is evaluated and not on spin of particle. To include the physics of spin polarization the use of a spin-polarized density functional for the exchange and correlation is required. Thus the particular method used for this purpose is called the local spin density approximation (LSDA). The

local spin-density approximation (LSDA) is a straightforward generalization of the LDA to include electron spin, the expression is given by

$$E_{XC}^{LSDA}\ [n\uparrow, n\downarrow] = \int \epsilon_{XC}(n\uparrow, n\downarrow) n(r)\, dr \qquad (3.13)$$

where $\epsilon_{XC}(n\uparrow, n\downarrow)$ is the spin-dependent exchange-correlation energy density.

Lastly the DFT- LSDA with the ab-initio pseudopotential will be generated for atomic scatter centers. Since treatment of the many-electron system can be simplified further by introducing the pseudopotential concept, that stands for dividing the electrons of the atoms into core electrons and valence electrons and assuming that the core electrons only play a passive role, hence the ion-valence electron interaction is described in terms of pseudopotentials. The pseudopotential concept removes the core electrons and replaces the strong ionic potential by a weaker potential called the "pseudopotential".

3.1.2 Non-Equilibrium Green's Function (NEGF)

The basic idea of the NEGF-DFT technique is to use DFT to calculate the Hamiltonian and electronic structure of a device, use NEGF [41, 42] to determine the non-equilibrium quantum statistics that is needed to populate the electronic structure during current flow, and use real space numerical methods to handle the transport boundary conditions. The NEGF-DFT method provides a useful alternative and supplements to other atomistic techniques for analyzing spin-polarized quantum transport. The main advantage of the NEGF-DFT formalism is its close proximity to modern many body theories and quantum transport theory which is largely based on Green's functions. As such, new effects and new transport physics can be readily implemented into the NEGF-DFT theory. Furthermore, the NEGF-DFT method offers a simpler and more robust computational

alternative to existing atomistic techniques. In the NEGF implementation one has to have basis sets that separates the left and right semi-infinite leads in which the scattering region or the central region sandwiched between. It is also advantageous to have basis functions that only connect the nearest periodically repeated layers in the leads. The basis function sets employed in this thesis satisfy both of these conditions. The transport calculation has two steps. First the ground state density and potential are calculated self-consistently and then, using this self-consistent potential, the NEGF formalism is used to calculate the transmission as a function of energy. The transmission calculation, which consists of the calculation of the Green's function of the system in a suitable basis representation, will be considered. After the charge density is self-consistently converged, the transmission coefficients are calculated from standard Green's function methods. For each spin state σ, the transmission probabilities are calculated as

$$T_{\sigma}(E) = \Gamma_{r}[\Gamma_{L} G^{r} \Gamma_{r} G^{a}]_{\sigma} \qquad (3.14)$$

where G^{r} and G^{a} are the retarded and advanced Green's functions, Γ_{L} and Γ_{r} are the contact broadening functions associated with the left and right electrodes, respectively.

3.2 Software used for computation

The computational tools that are used to carry out the theoretical analysis are TRANSIESTA based Atomistic Toolkit software implementation code for performing electronic structure calculations. Python as a script language and Atomistic Tool Kit (ATK) is a versatile software platform for atomistic simulations of nanoscale systems.

3.2.1 TRANSIESTA

SIESTA (Spanish initiative for electronic simulations with thousands of atoms) [43] is a method and a software implementation for performing electronic structure calculation and ab-initio molecular dynamics simulations of molecules and solids. It uses a DFT code that predicts the physical properties of a collection of atoms. Properties that can be predicted using the code includes the Kohn-Sham band structures, electrons density, and Mullikan populations. Modern SIESTA code used for the study of transport properties is termed as TRANSIESTA. It utilizes inter atomic forces and stresses for structural geometry optimization. This method has diverse molecular dynamics options. It can be easily parallelized in a multi-mode cluster. The most unique feature of the method is its capability to treat large system with least hardware.

3.2.2 Python language and Virtual NanoLab

Python is an interpreted language, which can save you considerable time during program development because no compilation and linking are necessary. The interpreter can be used interactively, which makes it easy to experiment with features of the language [44]. Python allows writing very compact and readable programs.

A software platform for atomistic simulations of nanoscale systems has the following parts:

- **Atomistix Toolkit** (ATK)
  - State-of-the-art DFT engine for electronic structure and transport calculations.
- **Virtual NanoLab** (VNL)

- Modern graphic user interface GUI for setup and analysis.

➢ **NanoLanguage**

- Scripting language interface to ATK.
- Fully integrated in VNL.

The strength of ATK and VNL lies in their flexibility to describe systems of different symmetries. It can describe isolated systems (molecules), periodic systems (crystals), and system of the type bulk-nanodevice-bulk (two probe systems). Atomistic Toolkits (ATK) gives you access to a powerful set of modeling tools for investigating a variety of nanoscale systems such as molecules, bulk, and two-probe systems. The systems may contain nanowires, nanotubes, graphene, semiconductors, metals, etc.

Steps involved in a typical quantumwise simulation are given in appendix 1.

3.3 Sample Preparation and Computational Method Used

Our modeling includes preparation of theoretical samples of graphene based nanostructures. We have tried to model a set of D-shaped fully Zigzag (zGNAD) which are named as D_{11}, D_{12}, D_{13}, and, D_{14} and also mixed armchair zigzag graphene nanoantidots (azGNAD) with and without spin dopants as D_{21}, D_{22}, D_{23}, D_{24}. The deployment of D-shaping among these antidot structures helps us in achieving the spintronicity due to the rules of designing mentioned in Section 1.8. As shown in Figure (3.1) both sides of the central scattering region are connected to two semi-infinite electrodes (leads). The central scattering region has either D-shaped zigzag edge type of graphene nanoantidot (zGNAD) or mixed armchair and zigzag edges in the D-shaped graphene nanoantidot (azGNAD). The calculation of the complete system can be

obtained from two independent calculations of both electrodes regions and two probe calculations of the central scattering region. The electrode calculations are performed under periodical boundary conditions, with the unit cell being a single atomic layer along the ribbon axis. The sampling of Brillouin Zone integration is performed with a regular k point grid of $1 \times 1 \times 500$ mesh along with electronic relaxation. In our calculations, the exchange correlation potential is described by the local density approximation (LDA). A single-zeta (SZ) basis set is used and a mesh cutoff is taken to be 2040.855 eV. The simulation temperature is taken to be 300 K. In NEGF theory, the transmission function of the system is a sum of transmission probabilities of all channels available at the given energy under the applied external bias voltage. Besides, two-probe geometry consists of two semi-infinite systems coupled *via* a central scattering region. Thus in ATK, this geometry is broken down into three subsystems: the left electrode, the central region, and the right electrode. Thus in Figure 3.1 this division of the geometry is illustrated for a lithium single atomic chain which is the highly conducting nanoelectrode in the Z direction. The central region must include the part of the Li surfaces perturbed by the scattering region that is indicated in Figure 3.1 by a rectangular box. Beyond this box, the perturbation from the scattering region is screened out by the metallic leads of lithium and the effective potential retains its bulk value. Thus, the effective potential of the complete system can be obtained from two independent calculations of the electrode regions, and a composite of two-probe calculation of the central region that comprise of GNADs.

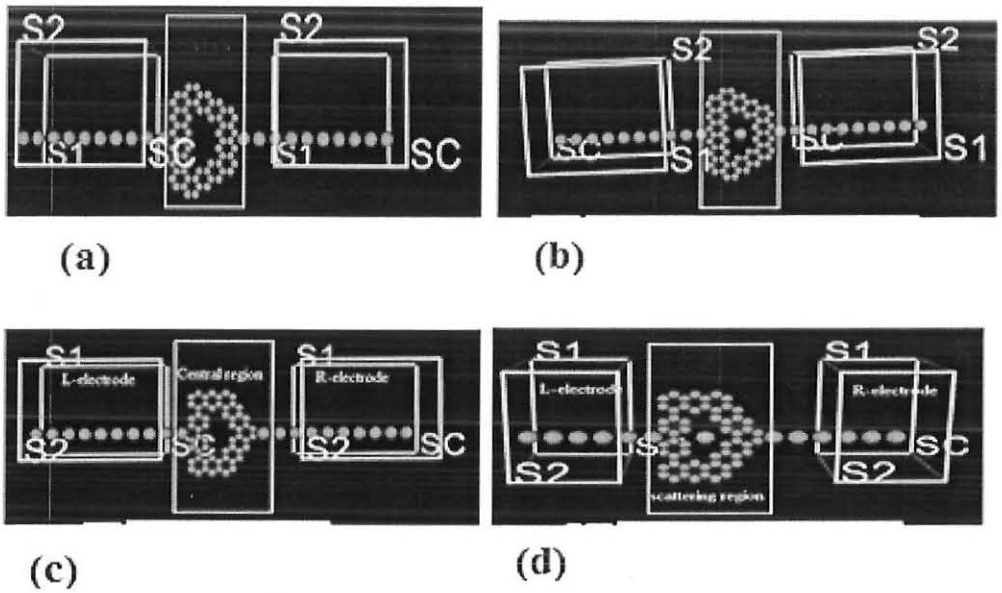

Figure 3.1 The two probes consists of two semi-infinite systems coupled *via* a scattering central region comprises of (a) Fully zigzag bare D-shaped graphene nanoantidot, D_{12} (b) Cobalt doped fully zigzag D-shaped GNAD device, D_{14}. (c) Bare mixed armchair-zigzag D-shaped graphene nanoantidot (azGNAD) structure, D_{22}. (d) Cobalt doped azGNAD in device structure, D_{24}. Note that in the case of (b) and (d) cobalt atom is placed at the center of GNADs. [The details of steps imperative for device fabrication are given in appendix 2].

CHAPTER FOUR

4. Results and Discussions

4.1 Modeling of Spintronics Structures

As discussed in Chapter 1, we can induce spintronicity among the graphene nanostructures either by magnetic doping or by cutting them into specific patterns like graphene flakes or antidot shapes. Here we are presenting our strategies of various theoretical sample syntheses for the spintronics applications. We have modeled D-shaped graphene nanoantidots (GNAD) devices of both bare and doped from pristine graphene sheet as zigzag graphene nanoantidots zGNAD, (D_{1x}) or (D_{11}, D_{12}, D_{13}, D_{14}) and, armchair-zigzag graphene nanoantidot azGNAD, (D_{2x}) or (D_{21}, D_{22}, D_{23}, D_{24}), respectively. We have attempted to connect these GNAD devices by symmetrical electrode contacts among the even named devices *viz* D_{12}, D_{14}, D_{22}, and D_{24}. In addition to this, asymmetrical electrode contacts are also modeled in the odd named devices *viz* D_{11}, D_{13}, D_{21}, and D_{23}, as discussed in Section 1.8, in the spintronic design rule No 3, the contact geometry asymmetry is also found to enhance spin currents.

4.1.1 Synthesis of symmetrically connected GNAD structures

The even named spin devices have lithium electrodes attached with the central graphene nanostructure (GNAD) in a symmetrical manner. From Figure 4.1 it is clear that for all the even devices, the electrodes are exactly placed at the center of the GNAD. Out of these four devices, Figure 4.1 (a) and 4.1 (c) illustrate the antidot structure without any effect of external dopant, and the contacts are also symmetrically placed. Hence we

expect that in these devices, the origin of spintronicity is only due to the design rule No 2 given in Section 1.8 which reinstates the net effects of the angular positions for the zigzag edge symmetry, moreover, we also expect the contribution of the external adatom for the spintronicity of the doped symmetrically attached GNAD.

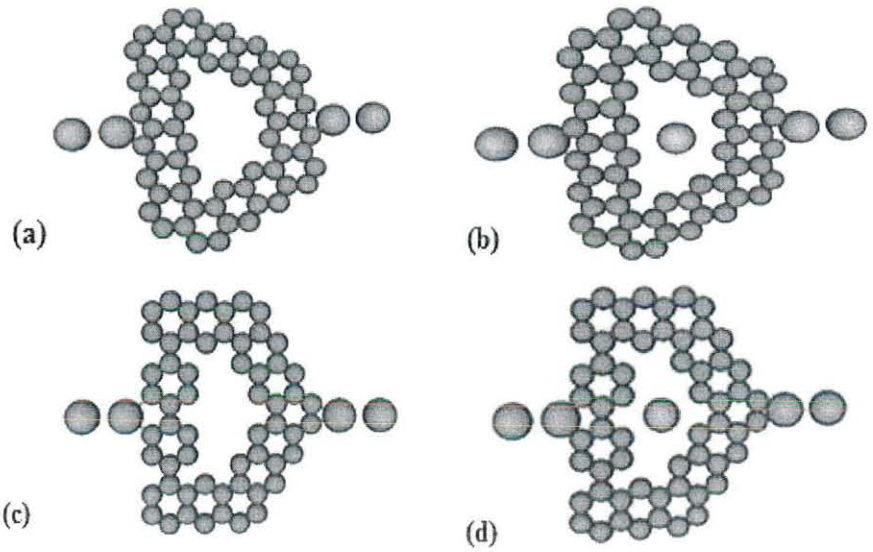

Figure 4.1 Electrode-device-electrode symmetrical contacts. (a) Bare zGNAD (D_{12}) (b) Co-doped zGNAD (D_{14}); the dopant atom is placed at the center of GNAD, (c) azGNAD (D_{22}), and (d) Co-doped azGNAD (D_{24}); the dopant atom is placed at the center of GNAD.

In our device modeling the two probes system basically consists of three main regions (the left, the right, and the central region). The left and right nanoelectrodes are constructed from lithium atomic chains while the middle region constructed from D-shaped zGNAD and/or azGNAD. It should be noted that the leads are semi-infinite, made up of highly ballistic and conducting lithium nanoelectrode. Each of these nanoelectrodes can act as a source and drain for the calculation of the electronic transmission. The high

conductivity of Li-chain is mainly ascribed to the band structure of the chain that is usually composed of $2\sigma^*$ bonding bands 2 doubly degenerate non bonding π bands and $2\sigma^*$ bands, in which doubly degenerate π and $2\sigma^*$ bands cross Fermi level leading to conduction channels giving 3 G_0 values of conductance ($G_0 = 2e^2/h$) and thus ballisticity happens [45]. Figure 4.1 (b) and 4.1 (d) shows the position of cobalt atom inside the two types of corresponding D-shaped GNADs. This helps in utilizing both the novel effects of edge symmetry as well as doping the unpaired electrons of Co atom in GNAD. The length of the central region of the entire D_{1x} type spin device (zGNAD) is 14.8 nm whereas that of D_{2x} type (azGNAD) is 23.9 nm, respectively, and thus the dopant Co atom is positioned exactly at the center of these respective lengths in the corresponding spin device in between the two electrodes. It is to be noted that the spin is injected from the left electrode of the device with a spin current polarization of 100% that stands for all the injected electrons having up spin. From Table 4.1 it is clear that all the devices have very low total energy of formation and thus they are highly stable with values of around -10^4 eVs.

Table 4.1 Total energy of devices with symmetrical contact

Devices Name	**Symmetrical nanocontact configurations**	**Total energy (eV)**
D_{12}	Bare zGNAD	-10133.97
D_{14}	Co-doped zGNAD	-11059.27
D_{22}	Bare azGNAD	-9200.82
D_{24}	Co-doped azGNAD	-10046.85

Table 4.1 summarizes total energy of formation of the symmetric devices. Thus doping enhances the stability of both D_{1x} and D_{2x} devices in the symmetrical contact. As we can see in the Table 4.1, from devices D_{1x}, D_{14} is more stable for its minimum energy of

formation. The effects of gating on the stability of these spin devices and the values of the spin population detected from the right electrode after the convergence of the DFT calculations is summarized in the Table 4.2. It has been found that the stability of the device decreases in general with the increase in external gate voltage. The decrease of stability is more for the application of negative biases in comparison to positive once. In addition, we have found unequal electron spin population in all the spin devices, as shown in Table 4.2.

Table 4.2 (a) The effect of gating on the total energy of symmetrical contacted devices D_{1x}

Sample	Gate Voltage	Total Energy (eV)	Total Charge(Spin Up)	Total Charge (Spin Down)	Charge Difference
D_{12}	0	-10133.97	136.340	123.67	12.67
	+1	-10133.64	136.390	123.44	12.95
	+2	-10133.11	136.400	123.25	13.15
	+3	-10132.44	136.350	123.12	13.23
	-1	-10132.52	135.770	124.31	11.46
	-2	-10128.77	136.340	123.87	12.47
	-3	-10126.41	136.650	123.71	12.94
D_{14}	0	-11059.27	140.740	128.26	12.48
	+1	-11058.94	140.830	127.98	12.85
	+2	-11058.38	140.795	127.82	12.98
	+3	-11057.64	140.798	127.64	13.16
	-1	-11058.20	140.260	128.82	11.44
	-2	-11054.12	140.720	128.42	12.30
	-3	-11051.65	141.110	128.21	12.90

(b) The effect of gating on the total energy of symmetrical D_{2x}devices

Sample	Gate Voltage	Total Energy (eV)	Total Charge (Spin Up)	Total Charge (Spin Down)	Charge Difference
D_{22}	0	-9200.820	123.940	112.16	11.78
	+1	-9200.620	123.720	112.23	11.49
	+2	-9200.160	123.680	112.11	11.57
	+3	-9199.550	123.650	111.97	11.68
	-1	-9198.710	124.740	111.32	13.42
	-2	-9195.630	124.150	112.12	12.03
	-3	-9193.640	123.860	112.59	11.27
D_{24}	1	-10127.74	128.230	116.68	11.55
	2	-10122.64	128.700	116.50	12.20
	3	-10120.32	128.370	117.00	11.37
	0	-10127.97	128.420	116.64	11.78
	-1	-10127.73	128.230	116.68	11.55
	-2	-10127.28	128.110	116.63	11.48
	-3	-10126.72	128.000	116.57	11.43

The higher value of up spin charges is always detected in comparison to the lower values of down spin charges. This points the possibility of these GNAD nanostructures for deployment in the nanospintronic devices.

4.1.2 Synthesis of asymmetric GNAD spintronic structures

From Figure 4.2 it is clear that for all odd named devices, the electrodes are slightly shifted vertically and connected asymmetrically to the central region. Figure 4.3 (a) and

4.3 (c) illustrate, the antidot structure without any effect of external dopant and the contacts are also asymmetrically placed.

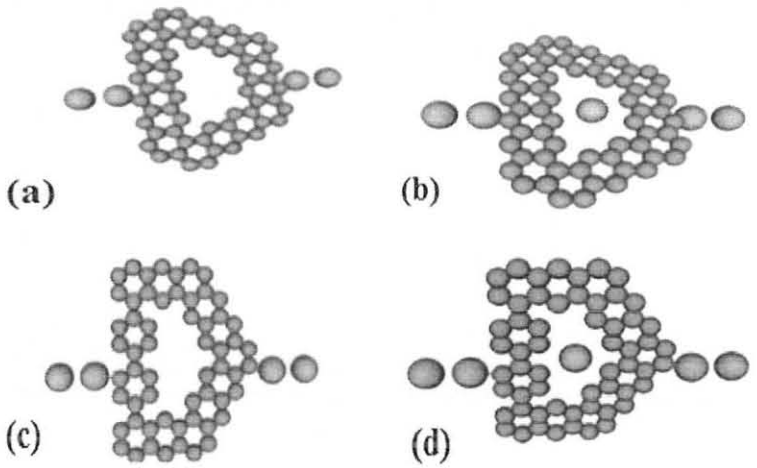

Figure 4.2Electrode-device-electrode asymmetrical contact configurations of four samples. (a) Bare zGNAD (D_{11}), (b) Co-doped zGNAD (D_{13}); the dopant atom is placed at the center of GNAD, (c) Bare azGNAD (D_{21}) and (d) Co-doped azGNAD (D_{23});the dopant atom is placed at the center of GNAD.

Hence we expect the origin of their spintronicity is due to the effects of zigzag edge symmetry angles as well as the asymmetrical contact of the Li electrode to the central region. The stability in asymmetrical electrode contact devices is almost similar to that in the symmetric contacts as shown in the Table 4.3. Nevertheless with the increase of asymmetry we can always expect more spintronicity from the devices.

Table 4.3 Description of asymmetrical devices with minimum energy obtained from self-consistent DFT calculations

Devices	Asymmetrical nanocontact configurations	Total Energy (eV)
D_{11}	Bare zGNAD	-10133.99
D_{13}	Co-doped zGNAD	-11059.29
D_{21}	Bare azGNAD	-9200.180
D_{23}	Co-doped azGNAD	-10127.99

From four odd named spin devices given in Table 4.3, the doped D-shaped GNADs are more stable compared to their undoped counter parts. However this stability varies with the external gate voltage as shown in Table 4.4.

Table 4.4 (a) The effect of gating on the total energy of D_{1x}devices with asymmetrical contact

Sample	Gate Voltage	Total Energy(eV)	Total-Charge (Spin Up)	Total Charge (Spin Down)	Charge Difference
D_{11}	0	-10133.99	136.330	123.78	12.55
	+1	-10133.71	136.410	123.52	12.89
	+2	-10133.23	136.400	123.35	13.05
	+3	-10132.59	136.390	123.18	13.21
	-1	-10132.84	136.600	123.58	13.02
	-2	-10128.67	136.340	123.97	12.37
	-3	-10126.32	136.700	123.77	12.93
D_{13}	0	-11059.29	140.930	128.30	12.63
	+1	-11059.08	141.010	128.05	12.96
	+2	-11058.63	141.030	127.84	13.19
	+3	-11058.03	140.950	127.73	13.22
	-1	-11057.98	140.400	128.90	11.50
	-2	-11053.99	140.890	128.48	12.41
	-3	-11051.46	141.320	128.27	13.05

Table 4.4 (b) The effect of gating on the total energy of asymmetrical contact D_{2x}devices

Sample	Gate Voltage	Total Energy(eV)	Total-Charge (Spin Up)	Total Charge (Spin Down)	Charge Difference
D_{21}	0	-9200.18	123.520	112.58	10.940
	+1	-9199.83	123.550	112.39	11.160
	+2	-9199.54	123.210	112.63	10.580
	+3	-9198.96	123.410	112.24	11.170
	-1	-9198.37	123.990	112.09	11.900
	-2	-9195.00	123.840	112.39	11.450
	-3	-9193.37	123.230	113.21	10.020
D_{23}	0	-10127.99	128.410	116.70	11.710
	+1	-10127.77	128.170	116.82	11.350
	+2	-10127.30	128.080	116.74	11.340
	+3	-10126.72	127.997	116.65	11.347
	-1	-10126.01	129.170	115.88	13.290
	-2	-10122.97	128.680	116.59	12.090
	-3	-10121.09	128.370	117.11	11.260

Here, we present view of the spin asymmetry in the conductance spectra by the plots of energy dependent relative spin polarization of the transmission probabilities, $\frac{T_{\uparrow} - T_{\downarrow}}{T_{\uparrow} + T_{\downarrow}}$ calculated for all samples. In all cases the net spin population is different from zero as shown in the Table 4.4. The summary of results of the effects of gating on the stability of asymmetrical spin devices and the values of the spin population detected from the right electrode after the convergence of the DFT calculations is given in Table 4.4 (a) and 4.4 (b). The stability of all these devices has the same trend as that of the symmetrical devices depicted in the Table 4.2.

4.2 Spin transmission from the symmetrically connected GNAD structures

We have calculated the spin transmission in the energy range of -2 eV to 2 eV for both the symmetrical and asymmetrical GNAD spin devices. The resulted transmission spectra along with the spin polarization curves which are calculated from spin transmission probability for the low energy electrons (Dirac fermions) are shown in the Figure 4.3. In the case of devices D_{12} and D_{22}, the transmissions of spin up electrons suppressed in the vicinity of the Fermi level, where the transmission of spin down density of electrons is maximum. Hence almost only spin down channel of the conductance spectrum observed near the Fermi energy between (-0.5 eV and 0.5 eV) as illustrated in Figure 4.3 (a) and 4.3 (b). This will be shown by a large transmission difference in the total transmission plot. When the two spin channels summed up, a very large unaffected net transmission is observed in the total transmission as shown in Figure 4.3 (c) and 4.3 (d) thus the polarization of the devices change. Unlike the recent report [30] on the spintronicity of the graphene flake, the overall polarization for the asymmetrical D_{1x} type devices decreases whereas for the D_{2x} type devices our result is consistent with this report. Thus our D_{1x} zigzag graphene nanoantidot device loses its spintronicity by the asymmetry contact.

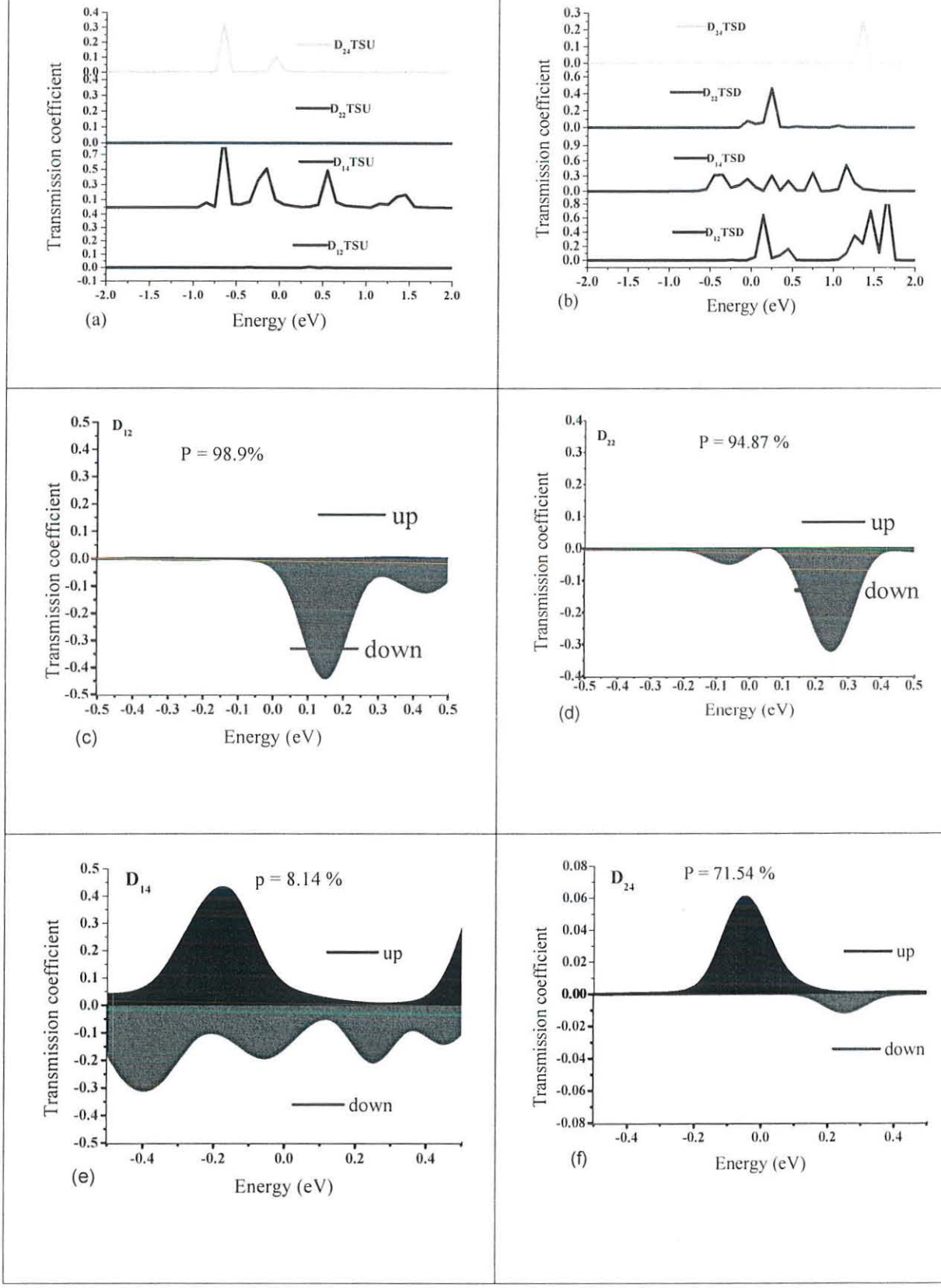
Transmission coefficient
Energy (eV)
(a)
D24TSU
D22TSU
D14TSU
D12TSU
(b)
D24TSD
D22TSD
D14TSD
D12TSD
(c)
D12
P = 98.9%
up
down
(d)
D22
P = 94.87 %
up
down
(e)
D14
p = 8.14 %
up
down
(f)
D24
P = 71.54 %
up
down

Figure 4.3 Plots of transmission spectra of symmetrical GNAD devices (a) spin up (b) spin down, (c) Spin polarization portrayed by the filled curves forthe bare D_{1x} and (d) Spin polarization portrayed by the filled curves forD_{2x}symmetric devices. It is to be noted that D_{14}andD_{24} are GNAD structures with cobalt atom placed at the central hollow region of GNAD. (TSU and TSD stand for the transmission spectra of the up spins and a transmission spectrum of the down spins respectively).

The simulation result of spin devices D_{14} and, D_{24}also shows that the transmissions of both spin up and spin down electrons are high. Hence the net spin density of electrons between up and down spin is small. When the two spin channels summed up, a very small unaffected net transmission can be observed in the total transmission. This is demonstrated by the total transmission plot in Figure 4.3 (e) and 4.3 (f). This minimum net transmission of the device degrades their polarization.

4.3 Spin transmission from the asymmetrical GNAD structures

In this section we are presenting our results from spin transmission calculations of the asymmetrically connected GNAD devices. The calculation range is set in between -2 eV to 2 eV in the vicinity of Fermi level. Figure 4.4 shows the transmission spectra along with the spin polarization results.

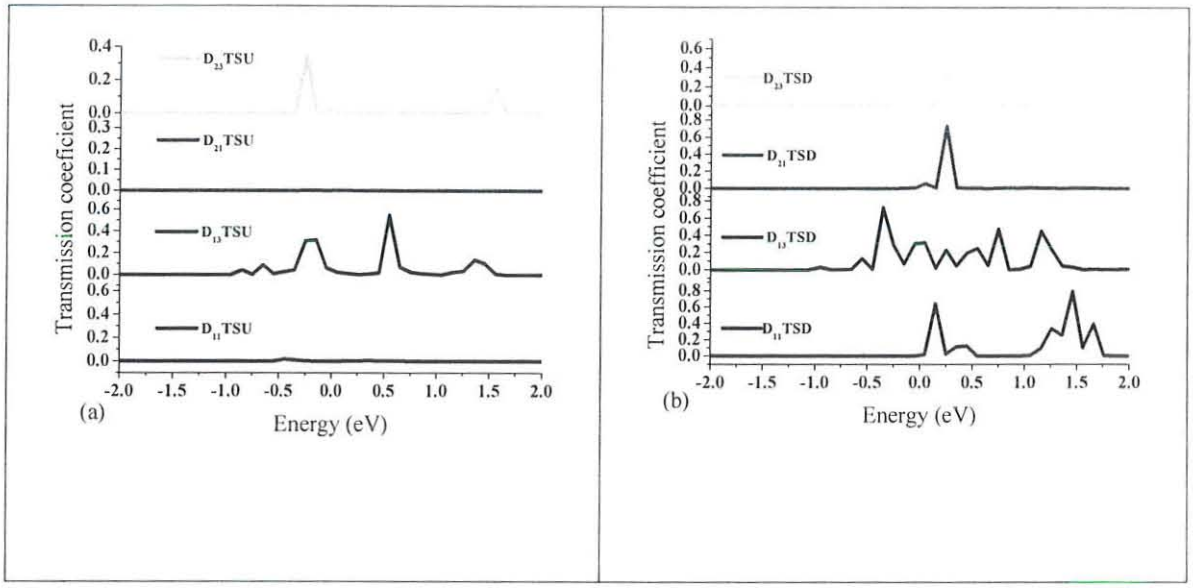
D23TSU
D21TSU
D13TSU
D11TSU
Transmission coeficient
Energy (eV)
(a)
D23TSD
D21TSD
D13TSD
D11TSD
Transmission coefficient
Energy (eV)
(b)

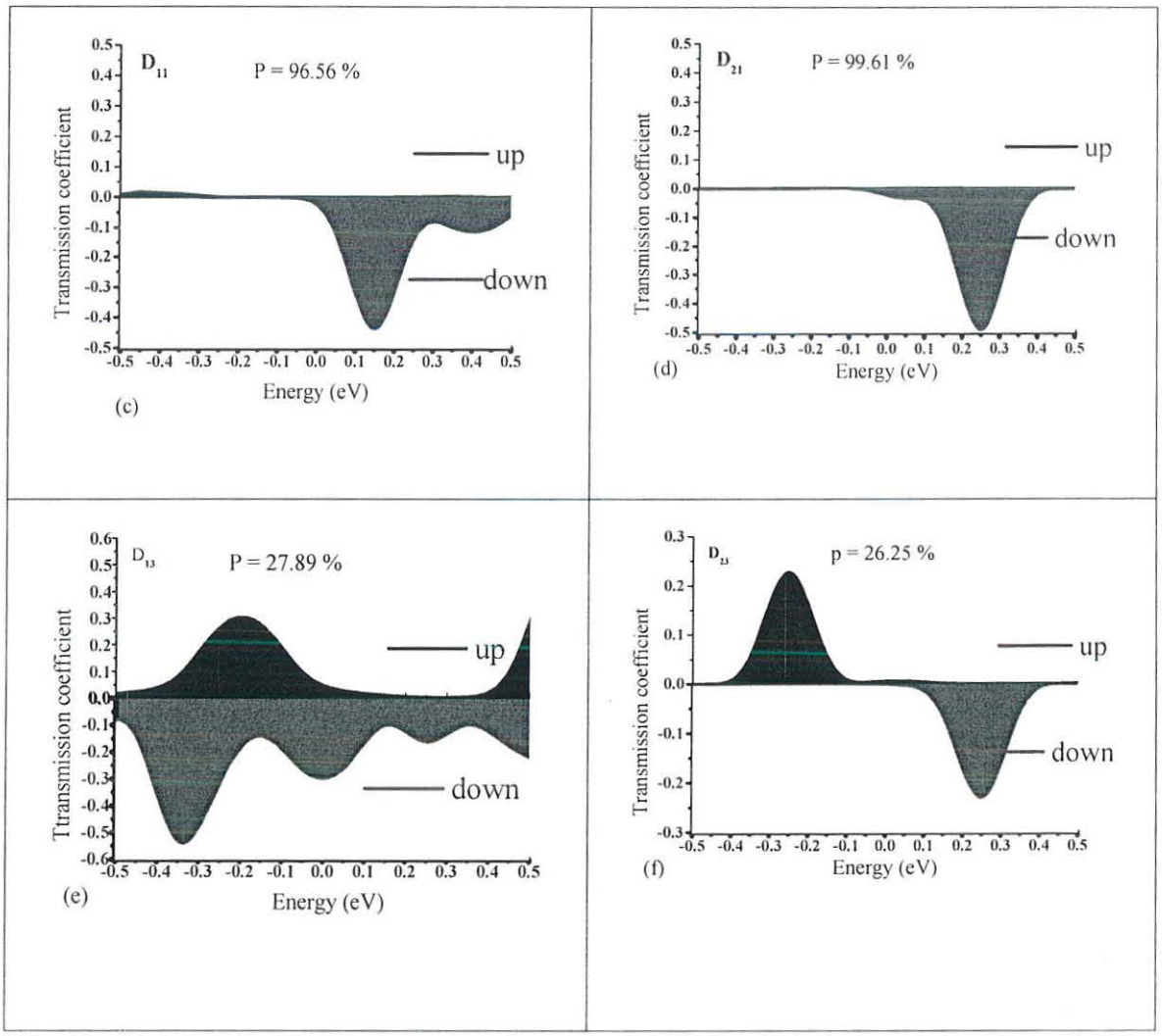
D11
P = 96.56 %
up
down
Transmission coefficient
Energy (eV)
(c)
D21
P = 99.61 %
up
down
Transmission coefficient
Energy (eV)
(d)
D13
P = 27.89 %
up
down
Ttransmission coefficient
Energy (eV)
(e)
D23
p = 26.25 %
up
down
Transmission coefficient
Energy (eV)
(f)

Figure 4.4 (a, b) Spin up and spin down transmission coefficients of asymmetric devices of the corresponding GNAD devices. Figure 4.4 (c, d, e, and f) spin polarization portrayed by the filled curves for the asymmetric devices.

The calculated zero-bias transmission spectra T (E) of asymmetrically connected devices are illustrated in Figure 4.4 (a) and 4.4 (b). In devices D_{11} and D_{21}, the transmission spectra of spin up electron are almost negligible whereas for the spin down large transmission spectra are observed and thus yield extreme polarization of the particular devices.

In the case of D_{13} and D_{23} spin devices the net transmission of spin up and spin down electrons near the Fermi energy between -0.5 eV and 0.5 eV is too small. This is demonstrated by the total transmission plot in Figure 4.4 (e) and 4.4 (f). When the two spin channels summed up, a very small unaffected net transmission can be observed in the total transmission. The reason behind is that in its ground state a Co atom inserted at the center of the hollow site has a magnetic moment antiparallel with the magnetic moments of the edge carbon atoms and AF magnetically coupled with the magnetic moments of edges states of the antidot, thus resulted in the minimum polarization effect of these devices.

In comparison to the contemporary theoretical reports [1, 40, 46] for the observance of the spintronicity among square, rhombus, hexagonal and triangular shaped antidots it is clear that these D-shaped especially those with no dopants exhibit almost double polarization values.

4.4 Origin and loss of spintronicity in doped and undoped systems in the two different contact configurations

From the spin polarization effect mentioned in the Section 4.2 and 4.3 it is clear that these novel D-shaped GNADs devices exhibit spintronic properties; however, the origin of this spintronicity is not mentioned in the previous sections. In this section we explore the possible cause that brings spintronicity in these novel graphene nanostructures. It is already ascribed that unbalanced net spin population among the zigzag edges are the main contributors for spintronicity. Hence we tried to analyze this aspect as we have only zigzag edges in D_{1x} devices and, both zigzag and armchair edges in the device D_{2x} where the armchair edge is in the direction perpendicular to the current flow as shown in Figure 4.5 and 4.6, respectively. First we present the results of spin injection among the various types of zigzag edges in the symmetrical GNAD devices with and without spin dopant. Next we will do the same for the asymmetrical configuration, and then the comparisons of the overall polarization among the devices in the symmetric and asymmetric configuration will be discussed in order to verify the dependence of polarization in the electrode-device contact position. The position of various carbon atoms and their respective zigzag edges are depicted in a Figure 4.5, and the net spin moment retained on these edges often the spin density functional theory self-consistency is summarized in Table 4.6.

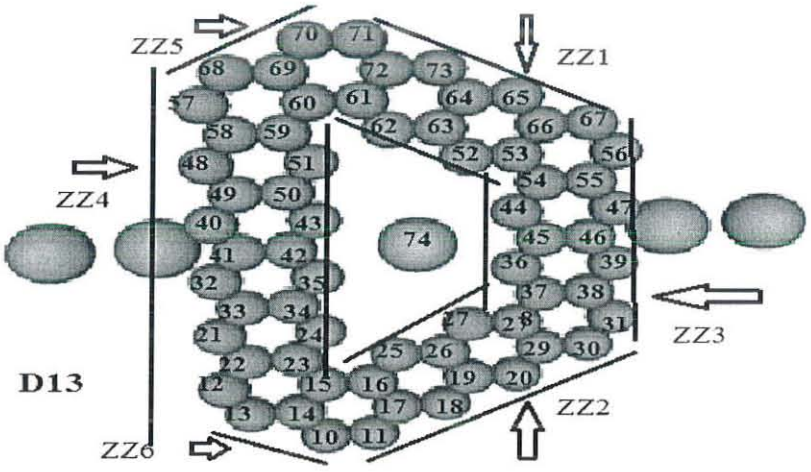

Figure 4.5: Devices (D_{1x} type) represent the edge effect on the spintronicity, where the central atom described by number 74 is Cobalt, and the two atoms at the right and left sides of the central region are parts of the semi-infinite Li electrodes.

The positions of atoms and types of edges are illustrated by the numbers and the black lines running along the inner and outer edges. For instance the inner edge corresponding to the outer edge ZZ_3 is $ZZ`_3$. The inner and outer edges of all the sides of the devices are named in the same fashion.

The fully zigzag edged device depicted in Figure 4.5 is prepared by using the aforementioned design rule, so that the outer zigzag edges ZZ_1, ZZ_3, ZZ_2, ZZ_6, ZZ_4, and ZZ_5 have lattice of type A, B, A, B, A, B, A, respectively. The angle among the (ZZ_1` $ZZ_2$, $ZZ_1$ZZ4, and $ZZ_2$ ZZ4) are 120°. In addition the inner edges $ZZ_1$`, ZZ_2`, $ZZ_3$`, and Z4` has a lattice of type B, B, A, B respectively. The angles between the inner zigzag edges ($ZZ_1$` ZZ_2`, $ZZ_1$` ZZ_4`, and $ZZ_2$` ZZ_4`) are 120°. Thus according to the generic design rule these edges are ferromagnetically coupled and hence we expect perfect spintronic nature from the device.

Table 4.5 The net magnetic moment of all devices without gate voltage

Names of a spin devices	Change in spin charge of the C atom of GNAD in the device				Net Magnetic momentof GNAD in μ_β
	Initial charge before SC		Final charge after SC		
	spin up	spin down	spin up	spin down	
D_{12}	256.00	0.00	135.56	122.57	6.495
D_{11}	256.00	0.00	135.40	122.74	6.330
D_{14}	265.00	0.00	140.14	127.00	6.570
D_{13}	265.00	0.00	140.76	126.43	7.165
D_{22}	232.00	0.00	122.93	111.03	5.955
D_{21}	232.00	0.00	122.33	111.52	5.405
D_{24}	241.00	0.00	127.37	115.84	5.765
D_{23}	241.00	0.00	127.08	115.72	5.680

The net magnetic moments demonstrated in the Table 4.5 reveals that all the samples given in the table have spintronic properties. The origin of the unbalanced spin population is found from analysis of individual edges of the devices as summarized further in the Table 4.6.

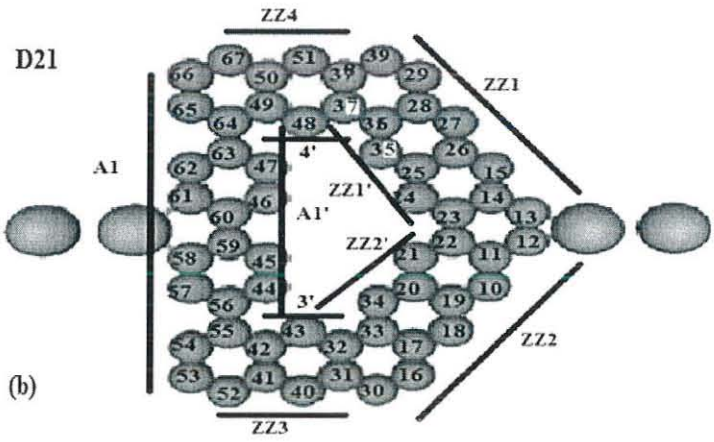

Figure 4.6: Devices (D_{2x} type) represent the edge effect on the spintronicity.

The normal to the consecutive sides of each zigzag edge around the device shown in Figure 4.6 are 60^{o} to each other both along the internal and external edges of it, moreover, the lattices along each consecutive edge is also of different type (for instance, for ZZ_4, ZZ_1, ZZ_2, ZZ_3, the lattice type on each edges are, B, A, B, A respectively, and the angle between each consecutive zigzag edges are 60^{o}) the same is true along the internal zigzag edges as well, However, although the design rule doesn't hold true for this device the first principle DFT calculation shows that the device indicates high spintronic behavior.

Table 4.6 Effects of the edges of asymmetrically configured devices on the polarization of the devices

sample	Edge	Charge before SC		Charge after SC		Polarization in %	Cutoff polarization
		Spin up	Spin down	Spin up	Spin down		High>5% ,no<2, 2%<low<5%
D_{11}	ZZ_1	28	0	15.15	12.96	7.780	High
	ZZ_2	28	0	15.11	13.01	7.600	High
	ZZ_3	28	0	14.70	13.95	2.590	Low
	ZZ_4	44	0	23.47	21.35	4.720	Low
	ZZ_5	12	0	6.010	6.054	0.358	No
	ZZ_6	12	0	6.020	6.050	0.277	No
	ZZ_1`	20	0	10.44	9.630	4.050	Low
	ZZ_2`	20	0	10.44	9.620	4.080	Low
	ZZ_3`	20	0	10.97	9.150	9.020	High
	ZZ_4`	44	0	23.29	21.01	5.160	High

D_{13}	ZZ_1	28	0	15.14	13.01	7.559	High
	ZZ_2	28	0	15.12	13.04	7.482	High
	ZZ_3	28	0	14.87	13.94	3.527	Low
	ZZ_4	44	0	23.58	21.20	5.309	High
	ZZ_5	12	0	6.120	5.930	1.538	No
	ZZ_6	12	0	6.110	5.940	1.418	No
	ZZ_1`	20	0	10.43	9.730	3.459	Low
	ZZ_2`	20	0	10.44	9.710	3.596	Low
	ZZ_3`	20	0	10.62	9.700	4.512	Low
	ZZ_4`	44	0	22.86	21.50	3.068	Low
D_{21}	ZZ_1	32	0	17.59	14.84	8.487	High
	ZZ_2	32	0	17.83	14.38	10.69	High
	ZZ_3	16	0	8.085	8.003	0.475	No
	ZZ_4	16	0	8.084	8.000	0.533	No
	A_1	56	0	28.39	28.50	0.194	No
	ZZ_1`	20	0	10.89	9.160	8.614	High
	ZZ_2`	20	0	10.88	9.170	8.528	High
	ZZ_3`	16	0	6.100	5.940	1.284	No
	ZZ_4`	12	0	6.080	5.950	1.076	No
	A_1`	12	0	8.400	7.560	5.261	High
D_{23}	ZZ_1	32	0	17.63	15.08	7.790	High
	ZZ_2	32	0	17.81	15.43	7.170	High
	ZZ_3	16	0	8.090	8.170	0.480	No
	ZZ_4	16	0	8.090	7.630	2.890	Low
	A_1	56	0	28.81	26.52	4.150	Low
	ZZ_1`	20	0	11.34	9.910	6.730	High
	ZZ_2`	20	0	10.48	9.890	2.870	Low
	ZZ_3`	12	0	6.050	5.590	4.030	Low
	ZZ_4`	12	0	6.070	6.080	0.150	No
	A_1`	16	0	8.160	7.910	1.540	No

From the self-consistent calculation results of D_{12} we have found that the two outer zigzag edges ZZ_1 and ZZ_2 that are parallel to the direction of transport, and the two inner edges of the nanoantidots $ZZ`_3$ and $ZZ`_4$ which are perpendicular to the transport direction provide high polarization effects; Whereas the remaining inner and outer zigzag edges contribute low spin polarized effects except ZZ_5 which doesn`t contribute any. The overall polarization of the D_{12} is then about 98.9% as shown in the Figure 4.3 (c). Similarly, from the simulation result of D_{11} we have obtained the two outer zigzag edges ZZ_1 and ZZ_2 which are parallel to the transport direction and ZZ_3 and ZZ_4 that are perpendicular to the transport direction show high polarization while ZZ_6 and ZZ_5 have no any polarization effect. In general the overall polarization of the particular device D_{11} is about 96.56%. The comparison between the polarization of individual zigzag edges of D_{11} and D_{13} shows that some of the edges on the D_{13} become depolarized due to dopant placed in it. The reason behind is that 0.763 charges are transferred to the antidot by cobalt and this charge poses the magnetic moment that is antiparallel to the magnetic moments of the edge states of particular antidot, thus the spintronicity of the devices loss.

Table 4.7 The total charge transferred from the Co atom to the antidots

Devices	**Total spin up (Co)**	**Total spin down (Co)**	**Total charge transferred to the antidots**	**Effects observed**
D13	5.48288	2.75522	0.76271	depolarization
D14	5.49949	2.71587	0.78464	depolarization
D23	5.42884	2.67842	0.88521	depolarization
D24	5.42928	2.68551	0.88521	depolarization

In general in both doped D_{1x} and D_{2x} devices the external magnetic atoms placed at the center of the devices transfer charge to them thus the antidots lose their spintronicity, this

is due to the fact that the charge transferred to the antidots owns magnetic moment antiparallel to the magnetic moments of some of the edges of the actual devices. The consequence of this result is clearly shown on the Table 4.6 and Table 4.8.

Table 4.8 (a) The effect of the inner and outer edges of Symmetrically connected D_{1x}devices on the spin polarization

Sample	ZZ edges	Initial charge		Final charge		Polarization in %	Cut off polarization 5%
		Spin up	Spin down	Spin up	Spin down		
D_{12}	ZZ_1	28	0	15.180	12.940	7.9650	High
	ZZ_2	28	0	15.200	12.920	8.1040	High
	ZZ_3	28	0	14.500	14.210	1.0200	No
	ZZ_4	44	0	23.370	21.380	4.4400	Low
	ZZ_5	12	0	6.0800	5.9800	0.8630	No
	ZZ_6	12	0	6.1300	5.9300	1.7080	No
	ZZ_1`	20	0	10.438	9.6100	4.1210	Low
	ZZ_2`	20	0	10.444	9.6300	4.0790	Low
	ZZ_3`	20	0	10.900	9.1600	8.6540	High
	ZZ_4`	44	0	23.300	20.990	5.2100	High
D_{14}	ZZ_1	28	0	14.500	13.640	3.0450	Low
	ZZ_2	28	0	14.680	13.800	3.0820	Low
	ZZ_3	28	0	15.280	13.130	7.5820	High
	ZZ_4	44	0	22.650	21.720	2.1620	Low
	ZZ_5	12	0	6.1000	5.9900	0.8460	No
	ZZ_6	12	0	6.5100	5.4700	8.6020	High
	ZZ_1`	20	0	11.070	8.9400	10.653	High
	ZZ_2`	20	0	10.140	10.060	0.4090	No
	ZZ_3`	20	0	10.640	10.090	0.2610	No
	ZZ_4`	44	0	23.030	21.620	3.1570	Low

Table 4.8 (b) The effect of the inner and outer edges of symmetrically connected D_{2x} devices on the spin polarization

sample	ZZ edges`	Initial charge		Final charge		Polarization in %	Cut off polarization 5%
		Spinup	Spin down	Spin up	Spin down		
D_{22}	ZZ_1	32	0	17.820	14.520	10.221	High
	ZZ_2	32	0	17.810	14.540	10.110	High
	ZZ_3	16	0	8.0731	8.0092	0.3981	No
	ZZ_4	16	0	8.0730	8.0091	0.3980	No
	A_1	56	0	28.690	28.260	0.7501	No
	A_1`	16	0	8.3600	7.6200	4.6090	Low
	ZZ_1`	20	0	10.953	9.0971	9.2560	High
	ZZ_2`	20	0	10.952	9.0969	9.2530	High
	ZZ_3`	12	0	6.1010	5.9350	13.828	High
	ZZ_4`	12	0	6.0980	5.9380	13.262	High
D_{24}	ZZ_1	32	0	17.786	14.6700	9.6098	High
	ZZ_2	32	0	17.787	15.3800	7.2750	High
	ZZ_3	16	0	8.0827	8.00505	0.4830	No
	ZZ_4	16	0	8.0829	8.00503	0.4840	No
	A_1	56	0	29.080	28.0500	0.1810	No
	A_1`	16	0	8.1470	8.14000	0.0002	No
	ZZ_1`	20	0	10.450	9.81300	3.0910	Low
	ZZ_2`	20	0	10.440	9.81100	3.1130	Low
	ZZ_3`	16	0	6.0450	6.01100	0.2790	No
	ZZ_4`	12	0	6.0480	6.00800	0.0330	No

The comparison between the polarization of edges of D_{12} and D_{14} devices provides a clear reason for the lose polarization of the internal edges ($ZZ`_3$ and $ZZ`_4$) of D_{14}. The

cause is that Co atom inserted at the center of the hollow site has opposite spin orientations to that of edge carbon atoms and AF magnetically coupled with the magnetic moments of edges states of the antidote. The same is true for D_{22} and D_{24}.

Table 4.7 (a) and (b) demonstrate the effect of dopant on the polarization of the individual edges of the symmetric devices. For instance the comparison between the edges of D_{22} and D_{24} shows that some edges which induces high polarization effect in D_{22}shows low or almost no polarization in D_{24} due to the dopant. In general putting cobalt adatom at the center of our D-shaped zGNAD structure diminishes the polarization of the device. In the case of D_{21} which has the same structure as D_{22} with small shift of electrode-device contact, the edges in ZZ_1, ZZ_2, $ZZ`_1$, $ZZ`_2$, and $A`_1$ (the inner armchair edge) shows polarization of 8.5%, 10.7%, 8.6%, 8.5% and 5.3% respectively. Moreover, zigzag edges $ZZ`_3$, $ZZ_4`$induce low polarization. For this nanostructure device we have obtained the overall polarization of 99.6% near the Fermi energy in between -0.5 eV to 0.5 eV. Recently researchers reported that the asymmetric electrode-device contact of rectangular nanoflake induces more spintronicity relative to its symmetric counterpart in the flake [30]. Our results also show the same trend with this result, unlike the D_{2x}devices. At exactly Fermi level the polarization slightly decreases for asymmetric D_{1x}. The comparison between D_{2x} devices shows that the polarization of the devices increases from symmetric D_{22} to asymmetry D_{21} and, the application of gate voltage also increase the polarization to 100%. However the dopant inserted at the internal vacant position of D_{23} and D_{24} degrades the polarization of the device as summarized in the Table 4.7.

4.5 Effects of Gating on the conductivity of the devices

From the analysis of these devices we have obtained the maximum polarization about 99.6% without the application of external gate voltage, however if one of the spin up or spin down channel is not completely insulated there is the possibility of leakage of small current in the spin devices. Hence in this thesis we try to use electric field with the help of gate electrode to completely insulate one of the spin channels in order to avoid linkage, so that the device will be 100% spin polarized and it could be used as a spin valve. Therefore in this section we will present the effect of gating on the devices by applying the external gate voltage ranging from -3 V to 3 V in the interval of 1 V.

4.5.1 Effects of gating on the conductivity of symmetric devices (D_{12}, D_{14}, D_{22} and D_{24})

In Table 4.8 the effect of gate voltage on the polarization of the symmetric devices is summarized. Although no significant effect is observed, generally, the applied external electric field reduces the polarization of D_{12} except for V_G = 1 V where polarization increases to 98.25%. In the case of D_{14} (the doped version of D_{12}) polarization increases with gate voltage.

Table 4.9 Effects of gate voltage on the polarization of devices symmetric to the electrode contact near the Fermi level at the energy window of 1 eV

Sample	Gate Voltage	Polarization in %		Sample	Gate Voltage	Polarization in %
D_{12}	0	96.56		D_{22}	0	94.87
	1	98.25			1	99.90
	2	89.71			2	89.73
	3	95.25			3	93.59
	-1	94.76			-1	100.0
	-2	73.41			-2	99.97
	-3	96.51			-3	100.0
D_{14}	0	8.778		D_{24}	0	71.54
	1	23.55			1	25.40
	2	30.20			2	11.29
	3	26.68			3	39.07
	-1	12.04			-1	75.51
	-2	41.93			-2	91.77
	-3	50.96			-3	1.78

The applied negative gate voltage enhances the polarization of D_{22} to 100%, however the polarization of D_{24} diminished for both positive and negative biased voltages except at the V_G = -1 V where polarization meaningfully increased to 91.77%. As the external gate voltage applied to the D_{12} device, the spin up channel insulated at V_G = -1 V where the spin down channel has the conductance of 0.15 G_0. Moreover maximum conductance of 0.8 G_0 is observed for the spin up channel where the spin down channel insulated at V_G = 1 V. Thus at -1 V and 1 V the pure SFET property of the device is observed. The activation of both conducting channels in this device is pragmatic at the gate voltages of -1.34 V and -0.13 V where the two channels cross each other, which represents the OFF states of switching device as shown in Figure 4.7 (a). Similarly we have obtained the maximum conductance of 0.9 G_0 when the V_G =2 V for device D_{14}as depicted in Figure 4.7 (b). The variation of conductance maxima between the two devices is the effect of the

external dopant used at the center of antidot D_{14}. The application of external electric field to this device enhances the conductance of spin up electron channel to 0.9 G_0 at gate voltage of 2 V where spin down electron density reads G = 0. Thus at 2 V the SFET property of the device is perfect. The activation of spin up and spin down channels in this device is practical at the gating voltage of -2.5 V where the two channels cross each other which represent OFF states of the switching device.

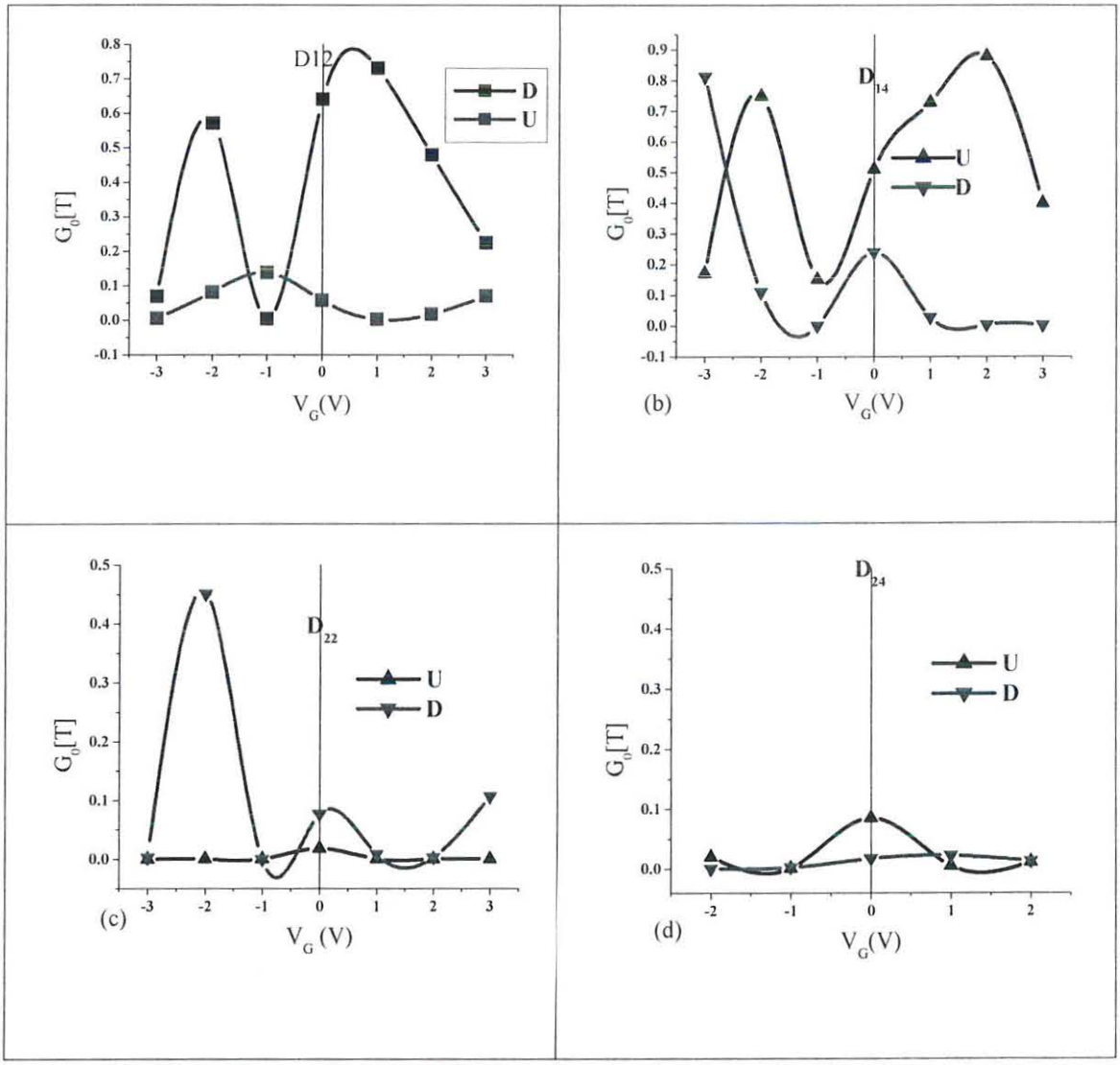

Figure 4.7 The effect of gate voltage on the conductivity of symmetrical devices at the Fermi level where U and D represents spin up and spin down respectively.

Device D_{22} and D_{24} are also induces spintronicity under the bias voltages for different conductance values. The applied external gate voltage changes the spin density of states near the Fermi level. Moreover, the presence of dopant in the devices suppresses the conductance of spin down electrons channel near the Fermi level for $V_G = 0$ as demonstrated in Figure 4.7 (c) and 4.7 (d).

4.5.2 Effects of gating on the conductivity of the devices in asymmetric contacts to the electrode

The gating effects on the up and down spin electron conductance spectra in the device D_{11} are shown in the Figure 4.8 (a). We obtained high density of down spin electrons at most of the gating voltages except for range of $-1.5\ V \leq V_G \leq 1\ V$ where the concentration of density of the spin up is more by about $0.1\ G_0$. The conductance of spin down electron channel reaches its maximum value of $0.7\ G_0$ for the gating of $V_G = 2$ V as depicted in the Figure 4.8 (a). It is to be noted that at this high value of down spin conductance the spin up channel is mostly insulated. Hence at the gate voltage of 2 V the Spin Field Effect Transistor SFET characteristic of this device is realistic. We can also see the activation of both channels in this device at the gating of -1.5 V as well as at 1 V, which signifies the OFF states of the switching device. Thus this class of materials allows only one type of spin to flow under the influence of certain specific electric field or gating voltage, and thus gives complete control over the spin polarization of current with higher efficiency for magnetic memory storage. Similarly, the effect of gating on the spin up and spin down electron conductance in the device D_{21} are shown in the Figure 4.8 (c). From this device we investigate that the conductance of spin up electron channel is insulated at almost all gate voltages. However the conductance of spin down electron is

maximum with the value of about 0.7 G_0 at zero gate voltage where the conductance of the up spin electron channel is completely insulated. The SFET characteristics of device D_{21} is accurate even without any external gate voltage as demonstrated in the inset of Figure4.8 (c). This interesting feature of the device is already mentioned in the previous section (Section 4.3) and its polarization is proven to be 99.61%. However the polarization rises to 100% for different values of gating. Hence we can also see the activation of both channels in this device at the gating of -3 V, -1.5V, -1V, 1V, 2 V, and 3 V, which represents OFF states of the switching device. Thus this device allows only one type of spin to flow under the influence of an electric field or the gating and thus gives complete control over the spin polarization of current. We also investigated that in D_{13} and D_{23} neither of the conducting channels blocked for both negative and positive external bias voltage. Hence the half metallic nature is not observed in these devices. This also coincides with their spin polarization calculated in the previous sections.

Table 4.10The effects of Gating on the polarization of the devices asymmetric to the electrode around the Fermi Level at 1 eV of the energy window

Sample	Gate Voltage	Polarization in %		Sample	Gate Voltage	Polarization in %
D_{11}	0	98.90		D_{21}	0	99.61
	1	97.89			1	81.34
	2	97.35			2	93.84
	3	95.94			3	99.53
	-1	75.71			-1	92.13
	-2	71.67			-2	99.13
	-3	96.03			-3	93.42

D_{13}	0	27.89	D_{23}	0	26.25
	1	11.72		1	5.805
	2	29.86		2	49.39
	3	55.98		3	51.34
	-1	5.615		-1	31.06
	-2	16.76		-2	84.02
	-3	30.16		-3	79.21

The effect of gating on the asymmetrically connected devices demonstrated in the Table 4.9 (for the case of D_{11} and D_{21}) disclose that the application of external gate voltage degrades the polarization of undoped asymmetrically connected devices, however in the case of the doped asymmetrically connected devices fluctuation of polarization is observed as shown in the same Table 4.9 (for the case of D_{13} and D_{23}). From the self-consistent simulation result of D_{21} and D_{23} we have realized that in the presence of dopant, the application of gate voltage highly affects the conductance of device as shown Figure 4.8 (c) and 4.8 (d).

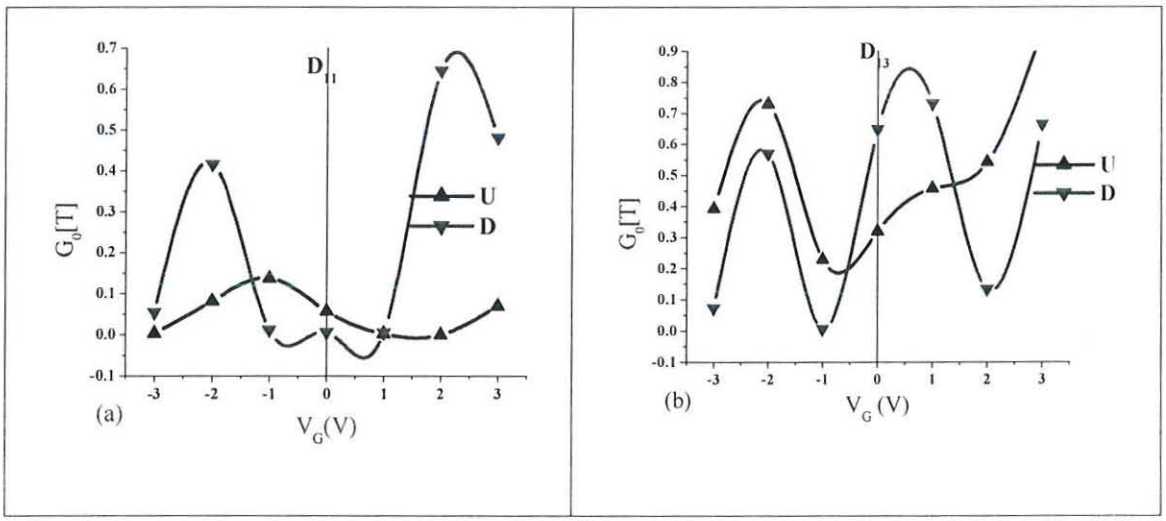

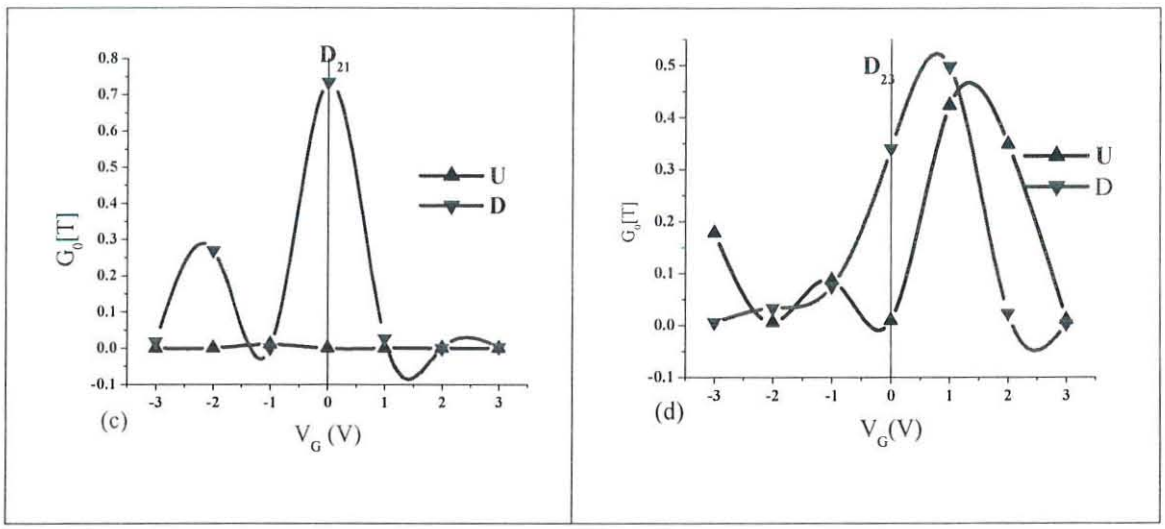

Figure 4.8 The effect of gate voltage on the conductivity of asymmetrically connected devices at the Fermi level where U and D stand for up and down spins respectively.

The application of external gate voltage enhances the polarization of some of our device to 100%. Hence we expect the particular devices would be used as the active spintronic materials for the future nanospintronic applications.

CHAPTER FIVE

Conclusion

The thesis is presenting spin transport properties among graphene nanostructures – which is otherwise a perfect material for spin less transport. Various design rules for the symmetry breaking among graphene nanostructures are discussed in the thesis for introducing spintronicity in the graphene. Some novel geometric conformation of graphene nanostructures are proposed in the thesis, which are promising for spin transport. For the first time we are presenting GNAD (Graphene NanoAntiDot) type of spin transistors, which are effective as spin valves. Ab-initio DFT in conjunction with NEGF theory is used to test our proposed spintronic GNAD models. Tricky GNAD sample modeling methods are discussed in the thesis for observing spin conductivities. The results of spin transmission among thesis nanostructures indicate the prominence of one of the spin transport channel in respect to the other channel for all of our sample models. The as observed spintronicity is explained with the help of various ZZ edges of the GNADs (D_{1x} and D_{2x}) and their spin contributions. The outer ZZ edges of GNADs are found to be more effective in instigating spin transport behaviors.

In this thesis-to the best of our knowledge-for the first time we performed a successful study on the spintronics properties of bare and doped D-shaped graphene nanoantidots. In addition, we have also investigated a perfect spintronic device (D_{12}) and obtained a very high the spin polarization value of more than 99.61% under non gated conditions.

From our studies we can conclude that on producing a lateral asymmetry among otherwise symmetric graphene nanoribbon edges, we can establish a strong spin-

dependency of the electron conductivity behavior resulting in the large spin polarization effects. This is shown by analyzing the GNADs' spin transmission behavior. Our results endorse that for the generating spin-polarized currents – symmetry breaking of the spin degeneracy of graphene sheet is required and this results in edge-localized states along the zigzag edges.

We have also found that with the applications of the gate voltages, the GNADs spin transport properties changes. Similarly, a change in the spin transport of the devices (D_{13}, D_{14}, D_{23} and D_{24}) is observed with presence of dopant Co atom. Furthermore the effect of electrode device contact configuration is also analyzed – the electrodes are contacted both symmetrically and asymmetrically to the devices' left-central-right region axis --and the result reveals that the spintronicity of D_{21}device enhances for the asymmetric contact as expected. However in the case of the asymmetric D_{22} device the reverse is true – the result is exceptional due to the fact that all previous reports indicate towards spin enhancement with contact asymmetry.

Energy dependent relative spin polarization of the transmission probabilities, $\frac{T_{\uparrow} - T_{\downarrow}}{T_{\uparrow} + T_{\downarrow}}$, is calculated for all the devices, and the minimum polarization of (8%) to maximum of 99.61% in the energy window of 1eV around the Fermi level is observed. The presence of a single Co atom at the center of both devices degrades their polarization capacity. In this work we have also investigated four promising devices D_{11}, D_{12}, D_{21} and D_{22} with high spintronic properties. The spin polarization of these devices is found to be 96.56%, 98.9 %, 99.61%, and 94.87%, respectively without the application of gate voltage; however the polarization of device D_{22} increases to almost 100% with the negative gate

voltages. Therefore, these graphene nanostructures can be considered as novel and a promising active material of spintronic devices without the need of ferromagnetic electrodes or other magnetic entities.

Unlike graphene nanoflakes the fully zigzag D-shaped GNAD depolarizes when asymmetrically connected to the electrode. This property is also one of the new findings we investigate in this research work. Hence the findings should be helpful in realizing carbon-based spin sources for spintronics.

In comparison to the contemporary theoretical reports for the observance of the spintronicity among square and triangular shaped graphene nanoantidots it is clear that our D-shaped GNAD specifically those with no dopant exhibit almost double polarization values.

Finally, yet importantly, the prospects of graphene based spintronic structures and the difficulties in realizing them are rightly elucidated in the thesis. The findings should be helpful in realizing carbon-based spin sources for spintronics.

References

1. Zheng X H, Zhang G R, Zeng Z, Garcia-Suarez V M, and Colin J L. (2009) Phys Review B 80:075413.
2. Wallace P R. (1947) Phys Rev 71: 622.
3. Novoselov K S, Geim A K , Morozov S V, Jiang D , Zhang Y, Dubonos S V, Grigorieva I V, and Firsov A A. (2004) Sci 306:5696.
4. Dubois S M M, Zanolli Z, Declerck X, and Charliera J C. (2009) Eur Phys J 71:00327.
5. Oleg V Y. (2010) Rep Prog Phys 73:056501.
6. Rozhkov A V, Giavaras G, Yury P B, Valentin F, and Franco N. (2011) Phys Reports 503:77.
7. Katsunori W, Ken-ichi S, Takeshi N, and Toshiaki E. (2010) Sci Tech Adv Mat 11:054504.
8. Maria A, and Vozmediano H. (2011) Phil Trans R Soc A 369:2625.
9. Ihn T, Güttinger J, Molitor F, Schnez S, Schurtenberger E, Jacobsen A, Hellmüller S, Frey T, Dröscher S, Stampfer C, and Enssli K. (2010) Mat today 13:44.
10. Max C L, Tim J E, Matthias B, and Heinrich K. (2007) Elec Dev Lett 28: 4.
11. Sudipta D, and Swapan K P. (2010) J Mat Chem 20: 8207.
12. Shou C Z. (1992) Int J Mod Phys B 6: 25.
13. Fujita M, Wakabayashi K, Nakada K, and Kusakabe K. (1996J) Phys Soc Jpn 65:1920.
14. Joseph E A, Daniel O, and Ruedi S. (2003) Phys today 31:38.
15. Krstajic P M, and Vasilopoulos P. (2011) J Phys Cond Mat 23:135302.

16. Phaedon A. (2010) Nano Lett 10:4285.

17. Sevinçli H, and Cuniberti G. (2010) Phys Rev B 81:113401.

18. Li T S, Huang Y C , Chang S C, Chang C P, and Lin M F. (2009) Phil Maga 89:697.

19. Hideki K and, Dai S H. (2008) J Phys Soc Jap 77: 044705.

20. Rycerz A. (2010) Phys Pol A 118:238.

21. Rosales L, Pacheco M, Barticevic Z, Leon A, Latge A, and Orellana P A. (2009) Phys Rev B 80:073402.

22. Zarbo L P, and Nikolic B K. (2007) Eur Phys Lett 80:47001.

23. Hossein K, Mahdi P, Meysam P, Rahim F, and Hans K.(2011) J Ele Chem Soc 158:213.

24. Yu-Ming L, Vasili P, Zhihong C, and Phaedon A. (2008) Phys Rev B 78:161409.

25. Hideki K, and Dai S H. (2008) J Phys Soc Jap 77: 044705.

26. Hu X Y, Tian H W, Zheng W T, Yu S S, Qiao L, Qu C Q, and Jiang Q. (2010) Chem Phys Lett 501:64.

27. An L, and Liu N. (2011) J Semi Con 32:052001.

28. Xiao-Fei L, Ling-Ling W, Ke-Qiu C, and Yi L. (2012) J Phys Cond Mat 24:095801.

29. Philip S, Yiming Z, and Mitch M. (2007) App Phys Lett 91: 042101.

30. Şahin H, and Senger R T. (2008) Phys Rev B 78:205423.

31. Cervantes-Sodi F, Csanyi G, Piscanec S, and Ferrari A C. (2008) Phys Rev B 77:165427.

32. Lieb E H. (1989) Phys Rev Lett 62: 1201.

33. PeresN M R, and Eduardo V C. (2007) J Phys Cond Mat 19:406231.

34. Laszlo P B, and Philippe L. (2010) Carbon 48: 2677.

35. Sheng W, Ning Z Y, Yang Z Q, and Guo H. (2010) Nano Tech 21:385201.

36. Yafei L, Zhen Z, Panwen S, and Zhongfang C. (2009) ACS Nano 3:1952.

37. Kevin T C, Neaton J B, and Marvin L C. (2008) Phys Rev B 77: 235430.

38. Li C, Decai Y, and Feng L. (2008) App Phys Lett 93: 223106.

39. Decai Y, Elizabeth M L, Miao L, Wei L, and Feng L. (2008) Nano Res1:2660.

40. Decai Y, Elizabeth M L, Miao L, Wei L, and Feng L. (2008) Nano Res 1: 497.

41. Brandbyge M, MozosJ L, Ordejón P, Taylor J, and Stokbro K. (2002) Phys Rev B 65:165401.

42. Stokbro K, Taylor J, Brandbyge M, and Guo H. (2007) Lec Phys 680: 2005.

43. Pablo O, Daniel S P, Alberto G, Emilio A, Javier J, and Jose M S. (2000) RIKEN Rev 29:42.

44. Manual A T K "A T K version 2008.10", Quantum Wise A/S (www.quantumwise.com) Retrieved Jan 2013.

45. Senger R T, Tongay S, Durgun E, and Ciraci S. (2005) Phys Rev B 72:075419.

46. Kumazaki H, and Hirashima D S. (2008) Low Temp Phys 34:10.

Appendix: 1

Steps involved in a typical quantumwise simulation

1. First, one needs to define and optimize the geometry of the system. For this task, VNL contains a database and several builders.

2. One should specify the details of the numerical calculator that should be used for the computation. This is done in VNL using the script generator or scripter for short.

3. The Script generator produces a Python script; it is recommended to always save it, for later reference. You may edit this script either in the internal editor or in any external text editor of your preference.

4. The script (symbolically denoted script.py) can be executed by dropping it on the Job manager, either directly from the instrument that created it, the Editor, or from the file system.

5. The data generated by ATK is stored in a NetCDF file which you specify in the scripter when setting up the calculation. The contents of the NetCDF file can be inspected in VNL by selecting the file in the file browser. A list of the objects contained in the file will then appear in the panel called result browser.

6. Build two-probe systems easily in the Atomic Manipulator. Cleave any crystal by specifying the Miller indices and surface cell. Align and rotate entire sample in the scattering region and control over the individual atoms positions, or delete/add atoms. Study transport properties of functionalized nanostructures, etc.

Appendix: 2

Steps imperative for device fabrications

1. At first, a common python script for building a zGNAD geometrical script is prepared by using standard graphene-ribbon.py in the script editor. Here the desired geometry of the zigzag antidot structure was set by carefully removing the carbon atoms from the nanoribbon. So that the final antidot in the form of D is obtained, such that all the edges of the D-shaped GNAD are made up of only zigzag GNR, thus the final geometry of zGNAD is obtained and optimized. It is to be noted that all the ZZ edges of the antidot are in the direction perpendicular to the circuit flow and they direct in the plane of the device as shown in Figure 3.1 (a). This implies that we always kept zero degree among zigzag edge angles. Hence, accordingly from the design rules, we can expect an unbalance spin moment of the C atoms in the direction of the current propagation in the device, which can pave the way for the investigation of spintronicity in this GNAD structure.

2. Similarly the user modified python script for azGNAD has been created as shown in Figure3.1(c) as per the design rules. It is clear from the Figure that an edge perpendicular to the device direction is armchair in configuration while the other entire are zigzags.

3. The as-prepared script dragged and dropped into nanolanguage scripter to set the required parameters and conditions in order to simulate density of state (DOS) and transmission spectrum (TS) in case of unbiased two probe system. Along with these two parameters current is added in case of biased two probe systems. Here basis set with single zeta type is set under method tab. Also for gated two probe system the voltages are

set across the central region in between -3 V to 3 V with an interval of 1 V while for equilibrium two probe system this voltage is set to 0 V. An NC file is created under the self-consistent tab. Finally, under analysis tab we defined the quantities DOS, Transmission spectrum in case of unbiased two probe system while along with these two, a parameter of gating is added in case of later two probe system to be computed from the converged electron density. The path to store the calculated result is given and this whole user modified python script is saved as a separate script.

4. The as-saved script for zGNAD band structure is run in ATK engines command window to carry out implementation and to calculate the desired results. As programmed executions terminated normally and a complete calculation file is obtained from the log window and is stored for further analysis. This file consists of huge data as it includes the initialization parameters, user defined conditions, geometrical description about the nanostructure system, and the coordinate values with respect to its dimensionality and most importantly the large iterative data of self-consistent calculations. The basic idea behind the self-consistent calculations is to calculate and compare the output values for the energies obtained after every successive iteration. This loop like process repeats itself continuously unless the difference between the two successive calculations becomes less than a default set value of energy and electron density accuracy. Once this state is attained the electron density gets converged and the energy gets minimized to attain the stability for the given nanostructure.

5. The VNL file in which the result is stored is visualized for the transmission spectrum and DOS plots. To see the value of gated results for the zGNAD two probe systems we have repeated the above mentioned process for the said values of gating.

6. The as calculated data for DOS and transmission spectrum is again extracted to origin for advanced analysis and their fine plots are obtained. Similarly, by extracting the value of gated data for each voltage combination on the electrodes, the gating characteristics for zGNAD are also plotted.